

Dear Dr. Howell, dear co-authors,

I note that all three reviewers had comments regarding the results presented in figure 7. Although in your responses you have already added some material (panel b), I suggest that you consider the opportunity to add more quantitative information about the lack of variability in the pixel surrounding the LiDAR site (either using a 3x3 window as suggested specifically by reviewer 3, or something that you think would be more appropriated).

At this stage, please, submit your revised manuscript with the edits you have shown in your responses.

Regards

Howell et al.

We have addressed all the concerns of the Reviewers and the result is a much-improved manuscript.

With regard to your comment we think we have already addressed that point about adding additional quantitative information about the lack of variability surrounding the LiDAR site. Specifically, we added aerial photography acquired over and beside the LiDAR site in 2012 (see Figure below from Scharien et al. (2014) that shows the aerial photograph coverage) and then compared those pond fraction estimates with the RADARSAT-2 peak melt pond fraction in 2012 when there was discrepancy between the LiDAR and the RADARSAT-2 pond fraction estimate. This comparison represents a wide area with about 861 samples. Figure 7b represents a distribution plot of this comparison showing how the melt pond fraction spatial variability surrounding the LiDAR site. We think that perhaps we were not very clear in the text describing this additional comparison and have revised the text in Section 3.2 as follows:

To give spatial context beyond the single point comparison at the LiDAR site, Figure 7b shows the distribution of RADARSAT-2 f_{pk} and the f_p determined from aerial photo observations on June 22nd, 2012 near Resolute. The aerial photographs were acquired within 1 week of f_{pk} coverage being observed at the LiDAR site. The comparison was done by averaging all RADARSAT-2 pixels within each aerial photo (123 photos) which represents ~861 samples. The mean aerial photograph f_p was 0.54 and RADARSAT-2 f_{pk} was 0.53 with an the RMSE of 0.10 and bias of 0. The distributions are in reasonably good agreement but RADARSAT-2 values are slightly narrower than the distribution of f_p from the aerial photographs. It is likely the RADARSAT-2 distribution is narrow on the left tail because our method captures peak pond coverage and some of the regions photographed were before or after their seasonal peak. We attribute the narrow right tail to the documented underestimation of equation (1) from Scharien et al. (2017). However, it is notable that both RADARSAT-2 and the aerial photograph datasets capture the same bimodal f_p distribution, with the first mode around 0.4-0.5 characterizing rougher sea ice areas and the second mode around 0.7 capturing smooth flooded sea ice.

Location of aerial photography:

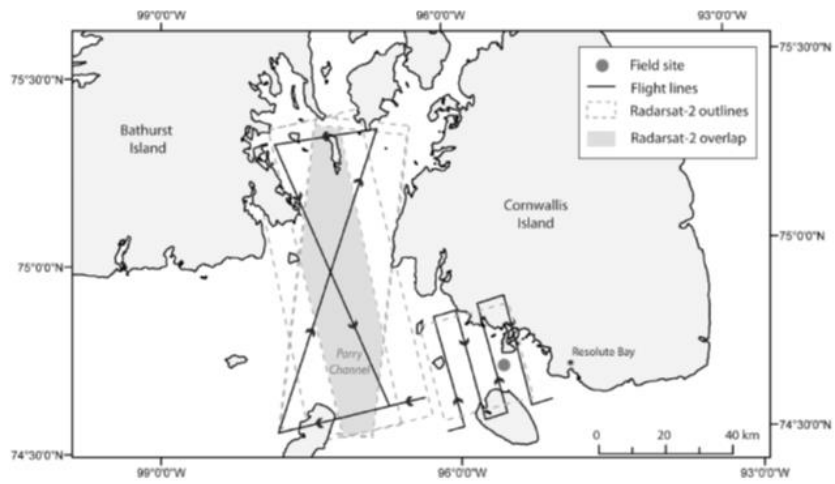


Figure 1. Map showing location of study area adjacent to the hamlet of Resolute Bay, NU, in the central Canadian Arctic Archipelago. Aerial photography flight lines over Parry and Field sites are shown along with outlines of 75 km × 25 km (Parry) and 25 km × 25 km (Field) Radsat-2 scenes. The shaded region over Parry denotes the overlapping portion of scenes acquired over the site.

Reviewer #1

Received and published: 10 August 2020

This manuscript uses RADARSAT-2 imagery to derive peak melt pond fraction values for sea ice in the Canadian Arctic Archipelago between 2009 and 2018. The basic method for deriving peak pond fraction was developed in an earlier publication, and this work applies that method to a larger dataset from a different satellite. The manuscript is well written and has only a few grammatical errors that are noted below. The results presented offer valuable insight into sea ice trends and variability in the CAA. However, there are a few issues with the validation of the RADARSAT-2 derived data that should be fixed or clarified prior to publication.

Howell et al.

We thank this reviewer for her/his comments that have improved this manuscript considerably. We have incorporated almost all of her/his suggestions.

Reviewer #1

General Comments

You define f_p as melt pond fraction. Throughout the paper you also use f_p to refer to peak melt pond fraction calculated from RADARSAT-2. It would improve clarity to separate the notation for these two different parameters.

Howell et al.

Very good suggestion. We have chosen to define peak melt pond fraction as f_{pk} and have changed the text throughout the manuscript to reflect this new notation.

Reviewer #1

There are two issues with the in-situ comparison:

1. The spatial footprint of the LiDAR scans from Landy et al., (2014) are small in comparison to the 100m resolution of RADARSAT-2 data used. These in-situ datasets would only cover 1-2 pixels in the radar image. Does this area represent the whole region? Perovich (2002) determined the aggregate scale (area at which a sample can be considered representative of the larger region) at SHEBA to be multiple kilometers. If the aggregate scale is much lower in the CAA (more homogeneous ice cover) this should be discussed.

Howell et al.

It is true the LiDAR areas would cover only ~1-2 pixels, however we only compared the LiDAR pond fraction to the ~1-2 RADARSAT-2 pixels directly coincident with the site. Therefore, we are not validating RADARSAT-2 melt pond fraction against a spot LiDAR *in situ* measurements, we are just validating the entire 100 m LiDAR melt pond fraction directly at the sampling site. In this case, it does not matter whether the *in situ* samples are representative of the aggregate scale.

We have clarified this in text so other readers to confuse other readers:

Revised Section 3.2

Figure 7a compares the time series of the entire 100 m LiDAR f_k coincident with the f_{pk} determined from RADARSAT-2 at the coinciding pixels.

Reviewer #1

2. Two in-situ samples are not enough to assess the accuracy of this method given the error presented in Figure 7. Here the prediction for 2011 is correct and the prediction for 2012 is not. On line 180 you state that the error is 0.1, but it looks more like 0.2 in the figure. Have you considered other in-situ datasets? For example, the three years of melt pond fraction timeseries observed on landfast ice near Utqiagvik, AK described in Polashenski et al., (2012)?

Howell et al.

We are limited by the scarcity of *in situ* melt pond fraction observations in the CAA and would have used more if we could. Moreover, finding observations that coincide with peak pond fraction further adds to the scarcity problem and the MODIS analysis was attempt to alleviate this problem. Unfortunately, we cannot use the *in situ* melt pond fraction dataset from Polashenski et al. (2012) because our RADARSAT-2 data only has consistent coverage in the Canadian Arctic waters in accordance with the operational domain of the Canadian Ice Service and therefore the Chukchi Sea is not covered. Despite having only two *in situ* samples, they least cover a long temporal time period allowing us to test whether RADARSAT-2 picks out the seasonal mean pond fraction or peak pond fraction. However, we do have aerial photograph estimates of melt pond fraction obtained over and adjacent the LiDAR site in 2012 from Scharien et al. (2014), which we have made use of to compare with RADARSAT-2 f_{pk} estimates.

We have added a new Figure 7b with the aerial photograph data and revised the following sections:

Revised Section 3.2

Figure 7a compares the time series of the entire 100 m LiDAR melt pond fraction coincident with the f_{pk} determined from RADARSAT-2 at the coinciding pixels. For 2011, RADARSAT-2 f_{pk} corresponds to the end of stage I and beginning of stage II thus providing a very good representation of the seasonal peak of the f_p , when the melt pond control on heat uptake and ice decay, through the ice-albedo feedback, is greatest. For 2012, RADARSAT-2 f_{pk} also corresponds to the end of stage I and beginning of stage II but is ~ 0.20 lower than *in situ* f_p values. This is likely due to the short duration but very high maximum f_p of 0.78 in 2012 as Scharien et al. (2017) found that equation (1) sometimes underestimates very high f_p due to the low γ° signal associated with very smooth FYI.

Figure 7b shows the distribution of RADARSAT-2 f_{pk} and the f_p determined from aerial photo observations on June 22nd, 2012 near Resolute. The aerial photographs were acquired within 1 week of f_{pk} coverage being observed at the LiDAR site. The comparison was done by averaging all RADARSAT-2 pixels within each aerial photo. The mean aerial photograph f_p was 0.54 and RADARSAT-2 f_{pk} was 0.53 with an the RMSE of 0.10 and bias of 0. The distributions are in reasonably good agreement but RADARSAT-2 values are slightly narrower than the distribution of f_p from the aerial photographs. It is likely the RADARSAT-2 distribution is narrow on the left tail because our method captures peak pond coverage and some of the regions photographed were before or after their

seasonal peak. We attribute the narrow right tail to the documented underestimation of equation (1) from Scharien et al. (2017). However, it is notable that both RADARSAT-2 and the aerial photograph datasets capture the same bimodal f_p distribution, with the first mode around 0.4-0.5 characterizing rougher sea ice areas and the second mode around 0.7 capturing smooth flooded sea ice.

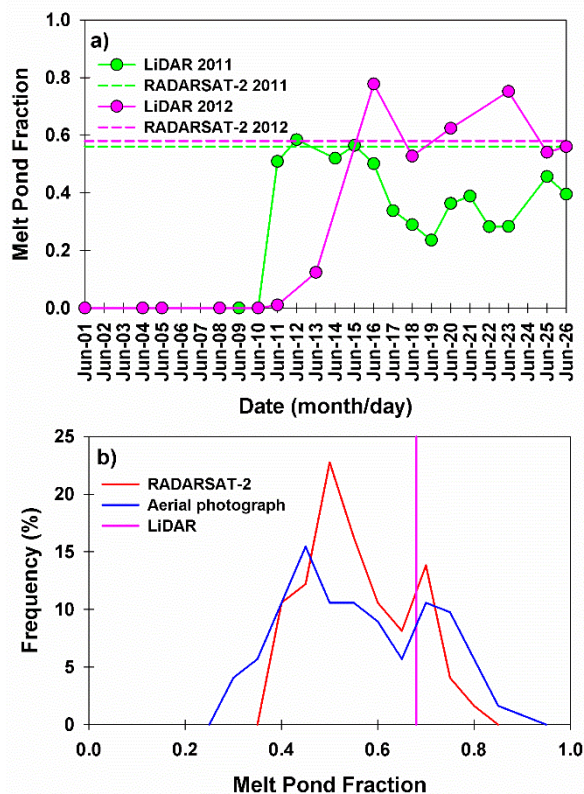


Figure 7. a) Temporal evolution of observed melt pond fraction (f_p) and RADARSAT-2 peak melt pond fraction (f_{pk}) at *in situ* observations sites for 2011 (74.7229°N; 95.1763°W) and 2012 (74.7264°N; 95.5772°W). b) Frequency distribution of RADARSAT-2 f_{pk} and aerial photograph f_p observations in Resolute Passage on June 22, 2012; the pink vertical link represents the mean LiDAR f_p on June 22, 2012.

Revised Section 2.1

Aerial photographs of estimated f_p directly over the LiDAR site and the adjacent sea ice area away from land and open water were also obtained on June 22, 2012. The aerial photographs have a pixel resolution 0.22 m resolution, cover 750 m by 750 m. In total, 123 aerial photographs of f_p were used and a complete description of the dataset is provided in Scharien et al. (2014).

Added Reference

Scharien, R. K., Hochheim, K., Landy, J., and Barber, D. G.: First-year sea ice melt pond fraction estimation from dual-polarisation C-band SAR – Part 2: Scaling *in situ* to Radarsat-2, *The Cryosphere*, 8, 2163–2176, <https://doi.org/10.5194/tc-8-2163-2014>, 2014.

Reviewer #1

Lines 183-194: What is the conclusion from the comparisons with MODIS? You note the reasons why RADARSAT-2 derived f_p and MODIS f_p could be misaligned (i.e. that the MODIS product is an 8-day average and peak ponding occurs on short timescales), and I am left with the impression that the MODIS data do not agree with your results. I would suggest expanding or clarifying the statistical analysis here. In Figure 8, both 2010 and 2011 make the RADARSAT-2 look statistically different than MODIS. The mean (blue line) of RADARSAT-2 is approximately equal to the max (top whisker) of MODIS.

Howell et al.

This is a good point raised by the Reviewer and we were not definitive in our wording based on the boxplots. The conclusion is that RADARSAT-2 pond fraction is higher on average than MODIS because the MODIS 8-day product is not representative of f_{pk} in the CAA. The weekly boxplots and max MODIS pond fraction boxplot all support this conclusion. We note that the box plot of maximum f_p from MODIS does capture some regions at peak during the 8-day time series. Another point is that MODIS estimation error needs to be acknowledged because although it is treated here as validation for the RADARSAT-2 f_{pk} estimates and rightly so but it has its own error component. We clarify this section in here as follows:

Revised Section 3.2

The seasonal time series of the 8-day composite MODIS f_p , the maximum seasonal MODIS f_p and the predicted RADARSAT-2 f_{pk} for 2009-2011 is shown in Figure 8. MODIS f_p observations within the CAA indicate initial pond formation occurred in May for all years with f_{pk} reached in mid-July for 2009 and in early June for 2010 and 2011. Compared to the RADARSAT-2 f_{pk} values, the peak MODIS f_p is ~ 0.20 smaller. RADARSAT-2 f_{pk} is higher on average than MODIS because the MODIS 8-day product does not represent f_{pk} . The MODIS f_p observations are determined weekly using 8-day composite image products that would include some melt pond formation and drainage processes prior-to, and after, the seasonal peak. Moreover, MODIS f_p observations give the time series of f_p therefore even the highest seasonal estimated MODIS f_p is reduced because while some regions of the CAA are at their seasonal peak but others are behind or ahead. To that end, we also calculated the maximum f_p from MODIS regardless of timing during the melt season, for each pixel, also shown in Figure 8. These values more closely compare with the RADARSAT-2 f_{pk} but are still ~ 0.05 smaller on average. Even the maximum f_p from MODIS is from an 8-day running mean of daily pond fraction estimates, so will underestimate the f_{pk} if the duration of peak ponding is < 8 days. However, the top whisker of the box plot of the maximum f_p from MODIS indicates that MODIS does capture some regions at peak during the 8-day time series. Although we are using MODIS f_p product to compare against our RADARSAT-2 f_{pk} estimates, Rösler et al. (2012) found that the MODIS f_p product also has errors up to ~ 0.1 . Overall, MODIS f_p estimates are more representative of the seasonal mean f_p rather than f_{pk} within the CAA.

Revised Conclusion

Based on our comparative analysis, RADARSAT-2 f_{pk} is more representative of peak f_p within the CAA compared to the MODIS 8-day product which on average was found to underestimate f_{pk} by ~ 0.2 and the is more representative of the seasonal mean f_p .

Reviewer #1

Specific comments

104 – Maybe this is covered in the Scharien paper, but is there a hypothesis for why this correlation exists? Is this method essentially just relating surface roughness (via radar backscatter) to peak pond fraction?

Howell et al.

Yes, it is explicitly covered and exploits the basic hypothesis that winter backscatter increases with increasing topography, for FYI, and increasing volume scattering, which is related to topography, for MYI. In each case, the increased topography leads to lower pond fraction, and visa versa. The high resolution optical imagery helps exploit this relationship. That is, using high spatial resolution optical imagery Scharien et al. (2017) were able to isolate internally coherent, and externally discrete, zones of sea ice in order to compare backscatter/texture and f_p and thus create simple models.

Reviewer #1

107 – If f_p is calculated directly from each radar pixel value (Eqn. 1), how does speckle filtering impact the f_p results?

Howell et al.

The impact of speckle filtering/not filtering was not assessed. As with most SAR images speckle is a problem with the goal being to obtain the most representative backscatter value for a local region (i.e. a cleaner image). The Lee facilitates this by smoothing the image without removing edges or sharp features in the images while minimizing the loss of radiometric and textural information. Although speckle filtering will change the f_{pk} results for specific pixels, it will not impact f_{pk} at the scale of the filter (i.e. within an x by x pixel area).

Reviewer #1

165 – If both sensors are the same frequency, why is there any difference here (Figure 6) (spatial resolution difference? Sensor measurement errors?)

Howell et al.

Good point. We should have provided some explanation for these differences

Revised Section 3.2

Frequency distributions of RADARSAT-2 f_{peak} and Sentinel-1 f_{peak} from Scharien et al. (2017) in the CAA for 2016 and 2017 are shown in Figure 6. Sentinel-1 appears to estimate more regions of lower f_{peak} compared to RADARSAT-2 which are typically associated with MYI. Whereas, RADARSAT-2 estimates more regions of higher f_{peak} which are typically associated with smooth FYI. We consider

these subtle differences to be primarily the result of taking the mean of all available April RADARSAT-2 imagery (Table 1) over all incidence angles in the CAA compared to only using images from Sentinel-1 within the CAA constrained to a certain incident angle range. As shown in Figure 2, the uncertainty in RADARSAT-2 f_{pk} varies depending on the number of pixel overlaps (images). Overall, the f_{pk} distributions are in good agreement between both sensors.

Reviewer #1

180 – this looks like it is 0.2 lower (difference between dashed pink line and peak pink dot). Am I reading this plot incorrectly?

Howell et al.

It should be 0.19 not 0.9. We have revised it ~0.2.

Reviewer #1

248 – “Slightly lower” is maybe an understatement? It is 20% lower. Either way, quantify the amount it is lower here.

Howell et al.

Revised Section 3.2

RADARSAT-2 f_{pk} was found to be in good agreement with the f_p maximum extent observed *in situ* for 2011 but was ~0.2 lower than 2012 when f_{pk} was very large (> 0.7) for a very short duration (1-2 days).

Reviewer #1

251 – In 214-231 you posit that the predictive power of this method only holds for landfast ice (i.e. when ice breakup is due to thermodynamics and not due to ice motion), how would this method be applicable to pan-Arctic estimates?

Howell et al.

In that case a Lagrangian tracking approach would be needed or the integrated melt pond fraction could be used with evolving sea ice extent. In both cases, significant testing would be required. We are working on this, but it is considerably outside the scope of this analysis.

Reviewer #1

Technical Corrections

59-61 – Run-on sentence.

Howell et al.

Revised Introduction

Model simulations have been utilized to understand the current and predicted future variability of sea ice conditions in the CAA (e.g. Dumas et al., 2006; Sou and Flato, 2009, Howell et al., 2016; Laliberté et al., 2016; Hu et al., 2018; Laliberté et al., 2018). However, modeling the CAA still remains challenging because complex sea ice dynamic and thermodynamic processes are often not accurately resolved in its narrow channels and inlets.

Reviewer #1

97 – "during April in within the CAA": Extra "in" here.

Howell et al.

Removed

Reviewer #1

152 – This sentence is unclear.

Howell et al.

Revised:

What is interesting in Figure 5a is that the mean RADARSAT-2 f_{peak} in 2009 was lower than all years from 2014-2018 (with the exception of 2016) despite the CAA containing less MYI area.

Reviewer #1

154 – "in addition" and "also" are redundant here.

Howell et al.

Removed "also"

Reviewer #1

161 – 3.2 header has extra "and". Also consider including oxford comma in this list for added clarity.

Howell et al.

Revised:

3.2 Comparison of RADARSAT-2 f_{pk} with Sentinel-1 f_{pk} , in situ f_p , and MODIS f_p

Reviewer #1

183 – Again a stylistic choice, but I find oxford commas to be helpful for clarity.

Howell et al.

Revised:

The seasonal time series of the 8-day composite MODIS f_p , the maximum seasonal MODIS f_p , and the predicted RADARSAT-2 f_{pk} for 2009-2011 is shown in Figure 8.

Reviewer #1

190 – "but" is an extra word here.

Howell et al.

Removed.

Reviewer #1

192 – Do you mean Figure 8 here?

Howell et al.

Yes. Changed to Figure 8.

Reviewer #1

215 – "The origin of the some of the ice" extra words here.

Howell et al.

Yes. Removed "the some of".

Reviewer #1

239 – "Overall, within the: : ": Revisit sentence structure here.

Howell et al.

Revised:

Overall, within the Viscount-Melville Sound region of CAA there is a period for which a significant statistical relationship exists between RADARSAT-2 f_{pk} and the summer ice area before sea ice dynamics degrades the relationship.

Reviewer #1

253 – "Was found to be excellent agreement": Missing "in" here.

Howell et al.

Added

"in".

Reviewer #1

249 – "maybe" should be "may be" in this context.

Howell et al.

Changed.

Reviewer #2

The manuscript uses RADARSAT-2 data to estimate melt pond fraction within the Canadian Arctic. The manuscript is clear and well written with figures clearly supporting the presented results and the discussion.

Howell et al.

We thank this reviewer for her/his comments that have improved this manuscript. We have incorporated almost all this reviewer's suggestions.

Reviewer #2

I found the investigation into the correlation between the different regions and the melt pond fraction one of the most important findings of this study. Maybe this finding could be more explicitly stated in the abstract and also in the conclusion? "Static/stable sea ice regions showed a higher detrended correlation." The mentioning of several regions is a bit vague.

Howell et al.

Agreed.

Revised Abstract:

Dynamically stable sea ice regions within the CAA exhibited higher detrended correlations between RADARSAT-2 f_{pk} summer sea ice area.

Revised Conclusions:

The results presented in this study indicate that dynamically stable sea ice regions within the CAA exhibit a higher detrended correlation between RADARSAT-2 f_{pk} and summer sea ice area.

Reviewer #2

Single pol RADARSAT-2 data was used, why is that? Was the combination of HH + HV lacking? Or did the HH-channel contribute sufficient information? This may have been covered in earlier work by e.g. Scharien et al., but would then be worth reiterating.

Howell et al.

Single pol RADARSAT-2 was used for two reasons. The first is that Scharien et al. (2017) found the HV data produced noisy results and the second there is not sufficient HV imagery in the early of the RADARSAT-2 to cover CAA. The latter is because only in the recent years has HH+HV been ordered operationally throughout the CAA.

Revised Data:

We limited our analysis to only RADARSAT-2 images at HH polarization because Scharien et al. (2017) found HV produced noisy results in addition to there not being sufficient imagery at HV polarization in the early period of the RADARSAT-2 record to cover CAA in April.

Reviewer #2

The in-situ area only covers areas with a relatively high proportion of melt ponds, were any other in-situ data available that could be used for the validation with a smaller proportion of melt ponds? Moreover, the area covered for the in-situ data is rather small compared to the pixel size of the RADARSAT-2 images. Are there larger datasets, either more locations or covering a larger area that could be used to strengthen the argument?

Howell et al.

Yes, we do have aerial photograph estimates of melt pond fraction obtained over and adjacent to the LiDAR site in 2012 from Scharien et al. (2014), which we have made use of to compare with RADARSAT-2 f_{pk} estimates. We have added a new Figure 7b with the aerial photograph data and revised the following sections:

Revised Section 3.2

Figure 7a compares the time series of the entire 100 m LiDAR melt pond fraction coincident with the f_{pk} determined from RADARSAT-2 at the coinciding pixels. For 2011, RADARSAT-2 f_{pk} corresponds to the end of stage I and beginning of stage II thus providing a very good representation of the seasonal peak of the f_p , when the melt pond control on heat uptake and ice decay, through the ice-albedo feedback, is greatest. For 2012, RADARSAT-2 f_{pk} also corresponds to the end of stage I and beginning of stage II but is ~ 0.2 lower than *in situ* f_p values. This is likely due to the short duration but very high maximum f_p of 0.78 in 2012 as Scharien et al. (2017) found that equation (1) sometimes underestimates very high f_p due to the low γ^p signal associated with very smooth FYI.

Figure 7b shows the distribution of RADARSAT-2 f_{pk} and the f_p determined from aerial photo observations on June 22nd, 2012 near Resolute. The aerial photographs were acquired within 1 week of f_{pk} coverage being observed at the LiDAR site. The comparison was done by averaging all RADARSAT-2 pixels within each aerial photo. The mean aerial photograph f_p was 0.54 and RADARSAT-2 f_{pk} was 0.53 with an the RMSE of 0.10 and bias of 0. The distributions are in reasonably good agreement but RADARSAT-2 values are slightly narrower than the distribution of f_p from the aerial photographs. It is likely the RADARSAT-2 distribution is narrow on the left tail because our method captures peak pond coverage and some of the regions photographed were before or after their seasonal peak. We attribute the narrow right tail to the documented underestimation of equation (1) from Scharien et al. (2017). However, it is notable that both RADARSAT-2 and the aerial photograph datasets capture the same bimodal f_p distribution, with the first mode around 0.4-0.5 characterizing rougher sea ice areas and the second mode around 0.7 capturing smooth flooded sea ice.

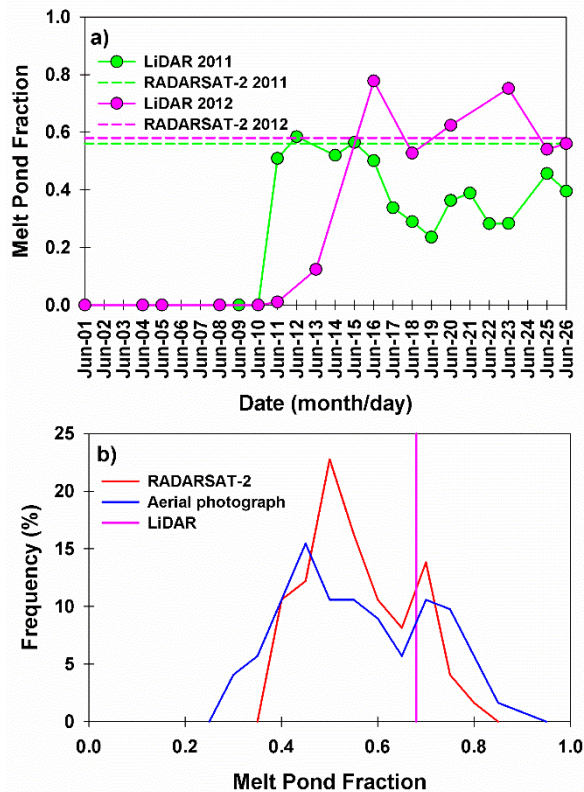


Figure 7. a) Temporal evolution of observed melt pond fraction (f_p) and RADARSAT-2 peak melt pond fraction (f_{pk}) at *in situ* observations sites for 2011 (74.7229°N; 95.1763°W) and 2012 (74.7264°N; 95.5772°W). b) Frequency distribution of RADARSAT-2 f_{pk} and aerial photograph f_p observations in Resolute Passage on June 22, 2012; the pink vertical link represents the mean LiDAR f_p on June 22, 2012.

Revised Data

Aerial photographs of estimated f_p directly over the LiDAR site and the adjacent sea ice area away from land and open water were also obtained on June 22, 2012. The aerial photographs have a pixel resolution 0.22 m resolution, cover 750 m by 750 m. In total, 123 aerial photographs of f_p were used and a complete description of the dataset is provided in Scharien et al. (2014).

Added Reference

Scharien, R. K., Hochheim, K., Landy, J., and Barber, D. G.: First-year sea ice melt pond fraction estimation from dual-polarisation C-band SAR – Part 2: Scaling in situ to Radarsat-2, *The Cryosphere*, 8, 2163–2176, <https://doi.org/10.5194/tc-8-2163-2014>, 2014.

Reviewer #2

The comparison between the results using Sentinel-1 and RADARSAT-2 imagery was interesting, but a discussion about why the results are different (e.g. Fig 6) is missing. Both of the images being C-band

SAR one would expect the results to align quite well. Please discuss this. The comparison between the RADARSAT-2 and MODIS data, particularly figure 8, seems to suggest large differences between the two sensors, where even the maximum f_p is significantly lower than the RADARSAT-2 estimates.

Howell et al.

We should have provided more discussion between and Sentinel-1 and RADARSAT-2 as also suggested by Reviewer #1.

Revised Section 3.2

Frequency distributions of RADARSAT-2 f_{pk} and Sentinel-1 f_{pk} from Scharien et al. (2017) in the CAA for 2016 and 2017 are shown in Figure 6. Sentinel-1 appears to estimate more regions of lower f_{pk} compared to RADARSAT-2 which are typically associated with MYI. Whereas, RADARSAT-2 estimates more regions of higher f_{peak} which are typically associated with smooth FYI. We consider these subtle differences to be primarily the result of taking the mean of all available April RADARSAT-2 imagery (Table 1) over all incidence angles in the CAA compared to only using images from Sentinel-1 within the CAA constrained to a certain incident angle range. As shown in Figure 2, the uncertainty in RADARSAT-2 f_{pk} varies depending on the number of pixel overlaps (images). Overall, the f_{pk} distributions are in good agreement between both sensors.

As for the MODIS product, it underestimates peak pond melt fraction in the CAA and is more representative of pond coverage at synoptic timescales. Even the maximum f_p from MODIS is from an 8-day running mean of daily pond fraction estimates, so will underestimate the seasonal peak f_p if the duration of peak ponding is <8 days. As also suggested by Reviewer #1 we firm up the wording here to point this out and have revised the text in 3.2 as follows:

Revised Section 3.2

The seasonal time series of the 8-day composite MODIS f_p , the maximum seasonal MODIS f_p and the predicted RADARSAT-2 f_{pk} for 2009-2011 is shown in Figure 8. MODIS f_p observations within the CAA indicate initial pond formation occurred in May for all years with f_{pk} reached in mid-July for 2009 and in early June for 2010 and 2011. Compared to the RADARSAT-2 f_{pk} values, the peak MODIS f_p is ~0.20 smaller. RADARSAT-2 f_{pk} is higher on average than MODIS because the MODIS 8-day product does not represent f_{pk} . The MODIS f_p observations are determined weekly using 8-day composite image products that would include some melt pond formation and drainage processes prior-to, and after, the seasonal peak. Moreover, MODIS f_p observations give the time series of f_p therefore even the highest seasonal estimated MODIS f_p is reduced because while some regions of the CAA are at their seasonal peak but others are behind or ahead. To that end, we also calculated the maximum f_p from MODIS regardless of timing during the melt season, for each pixel, also shown in Figure 8. These values more closely compare with the RADARSAT-2 f_{pk} but are still ~0.05 smaller on average. Even the maximum f_p from MODIS is from an 8-day running mean of daily pond fraction estimates, so will underestimate the seasonal peak f_p if the duration of peak ponding is <8 days. However, the top whisker of the box plot of the maximum f_p from MODIS indicates that MODIS does capture some regions at peak during the 8-day time series. Although we are using MODIS f_p product to compare against out

RADARSAT-2 f_{pk} estimates, Rösel et al. (2012) found that the MODIS f_p product also has errors up to ~0.1. Overall, MODIS f_p estimates are more representative of the seasonal mean f_p rather than f_{pk} within the CAA.

Reviewer #2

Were there regions in the CAA that showed better agreement between the MODIS and RADARSAT-2 estimates?

Howell et al.

Not really. We produced spatial maps but decided not to include them because they do not provide as much information as the boxplots.

Specific comments

Reviewer #2

Consider moving the information about stages of lake evolution on page 6 to the information about data or similar instead. Readers unfamiliar with melt pond development would be aided by an earlier introduction to the different stages. On P3 it is stated that the evolution stages covered by the field work covers 3 out of 4 stages, but on P 6 R177-179 it states that stage I and II was captured. Please clarify.

Howell et al.

We assume the reviewer means pond evolution. This seems the ideal place to describe these stages in accordance with the Figure 7 showing that the LiDAR site captures stages 1 to 3. Since the site is over first-year ice stage 4 will not occur and requires no discussion. We have removed references to the melt pond stages in the data description. Re-reading our text, it seems clear that the RADARSAT-2 f_{pk} values fall within end of stage I and beginning of stage II at the LiDAR site.

Reviewer #2

Is it expected that the environmental conditions remain reasonably stable in CAA during the month of April? If so maybe that could be added to strengthen the argument for combining RADARSAT-2 data for the analysis?

Howell et al.

Yes, it is expected. We have already explicitly stated this in the methodology: "...together with the fact that the majority of the sea ice in the CAA is landfast (immobile) during April which results in a temporally stable f_{pk} for all April images."

Reviewer #2

Minor comments

The use of the words excellent and good in the abstract are slightly abstract. Maybe it would be possible to provide some statistical measure?

Howell et al.

We added a statistical measure the temporal linkage but the spatial needs to be visual.

Revised Abstract

The temporal variability of RADARSAT-2 f_{pk} over the 10-year record was found to be strongly linked to the variability of mean April multi-year ice area with a statistically significant detrended correlation (R) of $R=-0.89$. The spatial distribution of RADARSAT-2 f_{pk} was found to be in excellent agreement with the sea ice stage of development prior to the melt season.

Reviewer #2

P2 L41. What is the difference between sea ice area and extent? Should it possibly say sea ice type and sea ice extent?

Howell et al.

No area and extent are the correct terms and the ones most commonly used. Sea ice area is ice concentration multiplied by the area of the region. Extent is also calculated as area multiplied by ice concentration but it this assumes that the area is 100% provided it is greater than a certain threshold (i.e. typically 15%). A great explanation is found on the NSIDC website “A simplified way to think of extent versus area is to imagine a slice of swiss cheese. Extent would be a measure of the edges of the slice of cheese and all of the space inside it. Area would be the measure of where there is cheese only, not including the holes. That is why if you compare extent and area in the same time period, extent is always bigger. A more precise explanation of extent versus area gets more complicated.”

[http://nsidc.org/arcticseaicenews/faq/#:~:text=The%20most%20common%20threshold%20\(and,said%20to%20be%20ice%20free.](http://nsidc.org/arcticseaicenews/faq/#:~:text=The%20most%20common%20threshold%20(and,said%20to%20be%20ice%20free.)

Reviewer #2

P2 L43. Does f_p here relate to maximum/mean values? Please clarify

Howell et al.

As suggested by Reviewer #1 we have modified the notation throughout the manuscript to denote melt pond fraction as f_p and peak melt pond fraction as f_{pk} .

Reviewer #2

P6. L169. Should it be : : : allows us to place the : : :?

Howell et al.

Yes. Inserted “to”.

Reviewer #2

P6. R192. Should this be Figure 8?

Howell et al.

Yes.

Reviewer #2

Fig 1. Please state what the green star indicates in the figure text.

Howell et al.

New Figure caption as follows:

Figure 1. Map of the Canadian Arctic Archipelago region (red shading). The green star indicates the location of the LiDAR and aerial photograph observations.

Reviewer #2

Fig 7. Should it be -W in the coordinates.

Howell et al.

Removed the ‘-‘

Reviewer #3

Received and published: 6 October 2020

This paper derives the melt pond fraction in month of April derived from Radarsat-2 imagery to predict the resulting sea ice area over the ensuing summer melt season within the Canadian archipelago, from years 2009-2018. The best results were found to be between stage of development in April and melt pond fraction, following the related paper by Scharien et al., 2017. Other comparisons were more challenging but were well explained. Due to my tardiness with this review, which I apologize for, I did read the other two reviews and the authors' response to both. I generally agreed with the reviewers comments and the responses were well posed. I will only add a couple of additional comments, that may be a little different.

Howell et al.

We have addressed all the Reviewer's comments. The MODIS spatial resolution suggestion was particularly useful for improving the manuscript.

Reviewer #3

1. Figure 7. As with the other two reviewers, I had some concerns with this figure, due to the relatively limited area of the lidar observations. The inclusion of the aerial photography and SAR comparisons that were added in Figure 7b are a valuable addition. Going back to Figure 7a, the Radarsat results themselves have no response to the changing melt conditions before, during and after. There is little change between the two years. Before the addition of Fig. 7b, I was thinking of not including it. I now wonder if they included a few more surrounding pixels to examine, like a 3X3 window, some variation might appear. How many R2 frames were examined during the field measurements periods?

Howell et al.

There is little variability using a 3x3 window near the LiDAR site and in this case we feel a direct one-to-one comparison is best. The individual RADARSAT-2 frames are averaged into a mosaic for the year and on average there are between 6 and 11 overlaps (Figure 2) with 8 in 2011 and 5 in 2012 over the LiDAR site. However, the point raised by the Reviewer is that it is important to mention uncertainty in the text and fewer pixel overlaps could also result in a reduction of the RADARSAT-2 peak pond fraction estimate. In 2012, the RADARSAT-2 peak melt pond fraction at the LiDAR pixel could be 0.1 higher according to Figure 2 which would be closer to the LiDAR values.

Revised Section 3.2 as follows:

This is likely due to the short duration but very high maximum f_p of 0.78 in 2012 as Scharien et al. (2017) found that equation (1) sometimes underestimates very high f_p due to the low γ^{ρ} signal associated with very smooth FYI. Another consideration is the uncertainty in RADARSAT-2 f_{pk} estimates is least 0.1 (Figure 2) which would bring the RADARSAT-2 f_{pk} values closer to the *in situ* values.

Reviewer #3

2. Section 3.2, first paragraph regarding R2 and Sentinel-1. Please add that S1 data collections for sea ice nominally also use HH polarization, same as R2. I am wondering about differences in the noise floor

and SNR between the two systems that may be leading to some of the differences seen in Fig. 6. Were an approximately equivalent number of images used by both sensors about the same or different, thinking about Fig. 2?

Howell et al.

We do not think it is a noise floor issue but rather it is an incident angle issue as we mention explicitly in the text. There were more Sentinel-1 images used to cover the CAA than RADARSAT-2 images but they were constrained to a certain incidence angle range. This was not possible with RADARSAT-2 and to create a close-to-seamless mosaic across the CAA with RADARSAT-2 we needed to take the average of the overlapping peak melt pond fraction values. Overall, the distributions are in very good agreement despite the different approaches.

Reviewer #3

3. Modis comparisons with R2, section 3.2 and Fig. 8. Please specify the resolution for the Modis products. What is the sensitivity of Modis to melt pond size? If one makes the assumption that Modis may not detect smaller ponds, that by itself may account for the differences seen in Modis Max pond fraction and R2 results, couldn't it? Also the 8-day composite of Modis may limit small pond fraction. Please clarify the impact of Modis resolution on pond fraction.

Howell et al.

This is a very good suggestion. By itself, the MODIS product spatial resolution is unlikely to be the primary cause since the temporal domain spans 8-days but the fact that the 12.5 km grid cell is made up of smaller 500 m pixels likely at different stages of pond evolution is another reason why the peak fraction is difficult to capture with MODIS. We have inserted another sentence into our revised the MODIS comparison.

Revised Section in 3.2:

Moreover, MODIS f_p values are essentially aggregated from 500 m clear-sky pixels within a 12.5 km x 12.5 km grid cell (Rösel et al., 2012) and the 500 m spatial resolution may limit detection of smaller pond fractions as well as not all of the 500 m pixels within the 12.5 km x 12.5 km grid cell are likely to be at the same melt pond stage evolution.

Revised Data and Methods:

Finally, we made use of 8-day composite satellite observations of f_p obtained from the MODIS Arctic melt pond cover fractions dataset that has a spatial resolution of 12.5 km for the period of 2009-2011 (Rösel et al., 2012).

Reviewer #3

4. Regarding Figs. 3 and 4 and Fig. 9 and 10. The relationship between stage of development and pond fraction was quite clear, shown in Fig.3-4. The greatest extent of low fractions were nearly all up in the northern CAA, with more variability, higher fractions in other areas. Then you come to Fig. 9 where any possible trend that one might expect in the MY/low fraction area in the north and in other regions

goes away. The authors explain the variations in A and B, in melt pond fraction/week of strongest correlation, by dynamics, southward transport of lower pond fraction ice. The patterns in Fig3-4 were so clear and then it becomes unclear, although there is some similarity in patterns between Viscount-Melville and McClintock in Fig. 10. It's all pretty interesting and rather surprising. I urge the authors to continue to investigate this topic. Perhaps the addition of ice motion drift can provide more insight.

Howell et al.

We agree and tracking the floes will likely improve the relationship which is something we are working on. Indeed, Viscount-Melville and the M'Clintock Channel have similar patterns because they have similar ice regimes (stagnant) so it is good to see agreement between them.

Spring melt pond fraction in the Canadian Arctic Archipelago predicted from RADARSAT-2

Stephen E.L. Howell¹, Randall K. Scharien², Jack Landy³ and Mike Brady¹

¹Climate Research Division, Environment and Climate Change Canada, Toronto, M3H 5T4, Canada

²Department of Geography, University of Victoria, Victoria, V8W 2Y2, Canada

³School of Geographical Sciences, University of Bristol, Bristol, BS8 1QU, United Kingdom

Correspondence to: Stephen E.L. Howell (Stephen.Howell@Canada.ca)

Abstract. Melt ponds form on the surface of Arctic sea ice during spring, influencing how much solar radiation is absorbed into the sea ice-ocean system, which in turn impacts the ablation of sea ice during the melt season. Accordingly, melt pond fraction (f_p) has been shown to be a useful predictor of sea ice area during the summer months. Sea ice dynamic and thermodynamic processes operating within the narrow channels and inlets of the Canadian Arctic Archipelago (CAA) during the summer months are difficult for model simulations to accurately resolve. Additional information on f_p variability in advance of the melt season within the CAA could help constrain model simulations and/or provide useful information in advance of the shipping season. Here, we use RADARSAT-2 imagery to predict and analyze peak melt pond fraction (f_{pk}) and evaluate its utility to provide predictive information with respect to sea ice area during the melt season within the CAA from 2009-2018. The temporal variability of RADARSAT-2 f_{pk} over the 10-year record was found to be strongly linked to the variability of mean April multi-year ice area with a statistically significant detrended correlation (R) of $R=-0.89$. The spatial distribution of RADARSAT-2 f_{pk} was found to be in excellent agreement with the sea ice stage of development prior to the melt season. RADARSAT-2 f_{pk} values were in good agreement with f_{pk} observed from *in situ* observations but were found to be ~ 0.05 larger compared to MODIS f_{pk} observations. Dynamically stable sea ice regions within the CAA exhibited higher detrended correlations between RADARSAT-2 f_{pk} and summer sea ice area. Our results show that RADARSAT-2 f_{pk} can be used to provide predictive information about summer sea ice area for a key shipping region of the Northwest Passage.

1 Introduction

Arctic sea ice extent during the summer months has declined considerably over the satellite record (Serreze et al., 2007; Stroeve et al., 2012; Peng and Meier, 2017). Surface melt ponds, which form on sea ice during the spring, play an important role in the decay of sea ice and seasonal reduction in ice extent because they influence how much solar radiation is absorbed into the sea ice-ocean system (Eicken et al., 2004). Specifically, the accumulation of meltwater on the surface of the sea ice lowers the albedo from ~ 0.8 to between 0.2-0.4 and enhances melt (Perovich et al., 2002). The topographical constraints over multi-year ice (MYI) imposed by hummocks typically result in MYI exhibiting a lower melt pond fraction (f_p) compared to seasonal first-year ice (FYI) (Grenfell and Perovich, 2004; Polashenski et al., 2012; Landy et al., 2015).

1 With Arctic sea ice transitioning from a MYI to FYI dominated icescape (Maslanik et al., 2011), the lower f_p of MYI will
2 gradually be replaced with the higher f_p of FYI, facilitating even more sea ice energy absorption and further enhancing sea
3 ice melt (Perovich and Polashenski, 2012).

4 Predicting the state of Arctic sea ice several months in advance is challenging and recently, the sea ice prediction
5 community has focused efforts on the development and utilization of dynamical forecast models (e.g. Chevallier et al., 2013;
6 Sigmond et al., 2013; Guemas et al., 2016). Despite these recent efforts, rapidly changing Arctic sea ice conditions will
7 continue to necessitate improved sea ice forecasting capabilities (Eicken, 2013). Accordingly, prognostic f_p schemes have
8 been integrated in climate models and have shown to exert a strong influence on summer sea ice area and extent (Flocco et
9 al., 2010; Flocco et al., 2012). Schröder et al. (2014) found a strong correlation between model-simulated May f_p and the
10 observed September sea ice extent. Observed f_p has also demonstrated significant predictive skill for September ice extent
11 from late-July onwards (Liu et al., 2015). However, while f_p estimates for the entire Arctic can be provided by model
12 simulations, more representative and higher spatial resolution observational estimates at regional and pan-Arctic scales are
13 much more difficult to obtain.

14 Optical remote sensing is the most widely utilized approach to estimate large-scale f_p from space (e.g. Markus et al.,
15 2003; Tschudi et al., 2008; Rösel et al., 2012; Istomina et al., 2014; Webster et al., 2015; Lee et al., 2020) but cloud cover
16 remains a significant problem. Techniques for retrieving f_p using advanced quad-polarization and compact-polarization mode
17 synthetic aperture radar (SAR) imagery, at C- and X-band frequencies, have also been developed (Scharien et al., 2014; Fors
18 et al., 2017; Li et al., 2017) but they are limited in systematic spatial application because the required polarization modes are
19 not always available from wide-swath imagery. However, using the winter backscatter from widely available Sentinel-1
20 SAR imagery, Scharien et al. (2017) recently demonstrated a technique for predicting spring peak melt pond fraction (f_{pk})
21 over the entire Canadian Arctic Archipelago (CAA) 3-4 months in advance of melt pond formation. These f_{pk} predictions
22 have potential utility in seasonal summer sea ice area and extent forecasts as early as April.

23 The CAA is a collection of islands located in Northern Canada (Figure 1) whose waterways are sea ice covered
24 between fall and spring. It is an active region for marine shipping and has recently experienced an increase in summer
25 shipping activity (Pizzolato et al., 2014). Model simulations have been utilized to understand the current and predicted future
26 variability of sea ice conditions in the CAA (e.g. Dumas et al., 2006; Sou and Flato, 2009, Howell et al., 2016; Laliberté et
27 al., 2016; Hu et al., 2018; Laliberté et al., 2018). However, modeling the CAA still remains challenging because complex sea
28 ice dynamic and thermodynamic processes are often not accurately resolved in its narrow channels and inlets. In addition,
29 the response of the CAA to climatic change is perhaps counter-intuitive as longer melt seasons are resulting in increased
30 MYI import from the Arctic Ocean during the summer months (Howell and Brady, 2019). Since f_{pk} is linked to summer sea
31 ice melt processes (e.g. Eicken et al., 2004; Skillingstad and Polashenski, 2018) additional information on f_{pk} variability
32 within the CAA could improve our understanding of regional summer melt processes, help constrain model simulations and
33 facilitate safer shipping activity in upcoming years.

1 In this study, we extend the work of Scharien et al. (2017) and investigate predicted f_{pk} variability within the CAA
2 over the longer-term record available from RADARSAT-2. Specifically, (i) we estimate f_{pk} in the CAA using RADARSAT-
3 2, (ii) evaluate the spatiotemporal variability of f_{pk} in the CAA from 2009-2018 (iii) compare RADARSAT-2 f_{pk} values to
4 Sentinel-1 f_{pk} values from Scharien et al. (2017), *in situ* f_p observations from Landy et al. (2014) and Moderate Resolution
5 Image Spectroradiometer (MODIS) f_p values from Rösel et al. (2012) and (iv) investigate the utility of RADARSAT-2 f_{pk} to
6 provide predictive information about sea ice area in the CAA during the summer melt season.

8 **2 Methodology**

9 **2.1 Data**

10 The primary dataset used in this analysis was 5.405 GHz (wavelength, $\lambda = 5.5$ cm; C-band) SAR imagery in
11 ScanSAR wide mode at HH polarization from RADARSAT-2 acquired over the CAA (Figure 1) in April from 2009-2018
12 (Table 1). RADARSAT-2 ScanSAR wide mode imagery has a spatial resolution of 100 m with an incidence angle range of
13 20.0° to 49.3°. We limited our analysis to only RADARSAT-2 images at HH polarization because Scharien et al. (2017)
14 found HV produced noisy results in addition to there not being sufficient imagery at HV polarization in the early period of
15 the RADARSAT-2 record to cover CAA in April.

16 *In situ* observations of f_p on landfast FYI were obtained in two consecutive years from sites in the CAA using a
17 terrestrial Light Detection and Ranging (LiDAR) system (Landy et al., 2014) (Figure 1, green star). In 2011, the site was
18 located in Allen Bay on FYI with relatively rough surface topography, whereas in 2012, the site was located in Resolute
19 Passage on FYI with relatively smooth topography. At each site, a time-series of f_p observations were collected within the
20 same 100 x 100 m area of the ice over a 2 to 3 week period following melt onset, covering three of the four stages of melt
21 pond evolution detailed in Eicken et al. (2004). The LiDAR system produces dense measurements over snow or sea ice with
22 specular reflection over melt ponds allowing melt pond fractions to be retrieved with an accuracy better than 5% (Landy et
23 al., 2014). These observations allow us to evaluate how well RADARSAT-2 resolves f_{pk} of seasonally-evolving sea ice
24 coverage.

25 Aerial photographs of estimated f_p directly over the LiDAR site and the adjacent sea ice area away from land and
26 open water were also obtained on June 22, 2012. The aerial photographs have a pixel resolution 0.22 m resolution, cover
27 750 m by 750 m. In total, 123 aerial photographs of f_p were used and a complete description of the dataset is provided in
28 Scharien et al. (2014).

29 Finally, we made use of 8-day composite satellite observations of f_p obtained from the MODIS Arctic melt pond
30 cover fractions dataset that has a spatial resolution of 12.5 km for the period of 2009-2011 (Rösel et al., 2012) and weekly
31 sea ice area and stage of development observations obtained from the Canadian Ice Service Digital Archive (CISDA)
32 regional ice charts for the period of 2009-2018 (Tivy et al., 2011).

34 **2.2 Estimating f_{pk} from RADARSAT-2**

1 RADARSAT-2 f_{pk} was determined using a modified approach to that described by Scharien et al. (2017). Their
 2 approach determines the second stage of the seasonal melt pond evolution cycle when f_p is at its peak (Eicken et al., 2003;
 3 Polashenski et al., 2012) using Sentinel-1 Extra Wide (EW) swath imagery obtained during April ~~in~~ within the CAA. April
 4 corresponds to late winter sea ice conditions in the CAA, when sea ice growth has reached its maximum and spring warming
 5 has yet to begin. Their approach was developed by relating the winter period HH gamma nought (γ°) backscatter in decibel
 6 (dB) from Sentinel-1 to f_{pk} observations in 1.7 m spatial resolution GeoEye-1 imagery, from spatially coincident image
 7 segments that represented homogeneous FYI and MYI regions. The result was that γ° can be converted to f_{pk} using the
 8 following equation:

$$9 \quad f_{pk} = -0.221 - 0.041(\gamma^\circ) \quad (1)$$

10 In equation (1), γ° was found to explain 73% of the variability in f_{pk} (Scharien et al., 2017).

11 In this study, all the available HH polarization RADARSAT-2 imagery over the CAA in April from 2009-2018
 12 (Table 1) were first calibrated to γ° which minimizes the influence of incidence angle more so than with sigma nought (σ°)
 13 (Small, 2011). RADARSAT-2 images were then speckle filtered using a 5x5 Lee Filter and spatially registered to a common
 14 map projection. Finally, γ° was converted to f_{pk} by applying Equation (1) to each RADARSAT-2 image. For each year, the
 15 corresponding RADARSAT-2 f_{pk} images in April were mosaicked together to cover the entire spatial domain of the CAA.
 16 Constructing a mosaic over a large region such as the CAA presents certain challenges with SAR imagery, particularly
 17 incidence angle variability. Even with the use of γ° , Scharien et al. (2017) found that because of varying incidence angles
 18 associated with different ScanSAR images that f_{pk} striping can still occur within the CAA in the mosaicked image. Our
 19 approach here was to average out incidence angle variability by taking advantage of large amount of overlapping
 20 RADARSAT-2 imagery within the CAA (i.e. 90 to 159 images; Table 1) together with the fact that the majority of the sea
 21 ice in the CAA is landfast (immobile) during April which results in a temporally stable f_{pk} for all April images. To produce a
 22 RADARSAT-2 f_{pk} mosaic within the CAA for each year, we calculated the mean f_{pk} for each overlapping pixel using all of
 23 each year's RADARSAT-2 April images that effectively helped to reduce f_{pk} striping across the CAA.

24 The root-mean square error (RMSE) of f_{pk} based on equation (1) is 0.085 (Scharien et al., 2017). While calculating
 25 the mean f_{pk} of the overlapping image pixels helps reduce striping across the CAA, it also adds additional uncertainty and its
 26 effectiveness depends on the number of overlaps. In order to quantify the additional uncertainty (RMSE_{R2}), we used the
 27 mean and maximum standard deviation of RADARSAT-2 f_{pk} of all pixels within the CAA calculated from 2009-2018 (f_{std})
 28 together with a range of pixel overlaps (n) in the following equation:

$$29 \quad \text{RMSE}_{R2} = [(f_{std}/n^{0.5})^2 + 0.085^2]^{0.5} \quad (2)$$

30 Since RADARSAT-2 imagery is acquired operationally, overlapping images vary interannually but pixel overlaps across the
 31 CAA were typically between 6-12. Figure 2 illustrates the RMSE_{R2} values for a range of pixel overlaps using the 2009-2018
 32 mean f_{std} value of 0.08 and the 2009-2018 maximum f_{std} value of 0.2. For the maximum f_{std} with pixel overlaps between 6-12
 33 the RMSE_{R2} ranges from 0.10-0.12.

1
2
3
4
5
6
7
8
9
10
11
12
13
14
15
16
17
18
19
20
21
22
23
24
25
26
27
28
29
30
31
32
33
34

3 Results and Discussion

3.1 RADARSAT-2 f_{pk} spatial and temporal variability from 2009-2018

The spatial distribution of mosaicked RADARSAT-2 f_{pk} and pre-melt season (i.e. April) and sea ice stage of develop conditions in the CAA for the 2009-2018 time period are shown in Figures 3 and 4, respectively. Lower f_{pk} values are located primarily in the northern regions of the CAA (Queen Elizabeth Islands), Viscount-Melville Sound and the M'Clintock Channel where the majority of the CAA's MYI is typically found. The shallow bays and narrow channels located throughout the CAA exhibit high f_{pk} values and these regions are typically associated with smooth FYI whereas rougher ice regions (i.e. Gulf of Boothia) are associated with lower f_{pk} values. We should expect a lower f_{pk} over MYI regions compared to FYI regions (Grenfell and Perovich, 2004; Perovich and Polashenski, 2012) and indeed the overall spatial distribution of RADARSAT-2 f_{pk} is in excellent agreement with the spatial distribution of sea ice stage of development prior to the melt season for all years.

Figure 5a shows the time series of RADARSAT-2 f_{pk} variability together with mean April MYI area in the CAA from 2009-2018. Over the 10-year record, the mean RADARSAT-2 f_{pk} was 0.47 and ranged from a low of 0.43 in 2009 to a high of 0.52 in 2013. The temporal variability in RADARSAT-2 f_{pk} is reflected in the variability of April MYI area within the CAA over the 10-year record with a statistically significant detrended correlation (R) of $R=-0.89$. The RADARSAT-2 f_{pk} linkage with April MYI area is particularly evident from 2011 and 2012 which were very light sea ice years within the CAA whereby a considerable amount of the CAA's MYI area was lost during the summer melt season (Howell et al., 2013) and this resulted in 2012 and 2013 (i.e. the years following extreme melt) being the two highest RADARSAT-2 f_{pk} years from 2009-2018 (Figure 3d-e). MYI area within in the CAA then increased following these light ice years and RADARSAT f_{pk} began to respond accordingly. In fact, there has always been a period of MYI recovery following light ice years with either MYI grown *in situ* and/or advected from Arctic Ocean into the CAA and gradually migrating to the CAA's southern regions (Howell et al., 2013). Figure 5b illustrates the standard deviation of RADARSAT-2 f_{pk} from 2009-2018 and spatially reflects the process of MYI flowing southward through the CAA as RADARSAT-2 f_{pk} was more variable in the MYI regions of the CAA compared to regions where FYI dominates the regional icescape.

What is interesting in Figure 5a is that the mean RADARSAT-2 f_{pk} in 2009 was lower than all years from 2014-2018 (with the exception of 2016) despite the CAA containing less MYI area. In addition, 2017 and 2018 ~~also~~ exhibited a larger spatial coverage of MYI compared to 2009 (Figure 4a, 4i-j). We suggest that higher RADARSAT-2 f_{pk} in recent years is a result of Arctic Ocean MYI entering the CAA being younger and thinner than in 2009 (Howell and Brady, 2019) with smoother surface topography, thereby having a higher summer melt pond coverage (Landy et al., 2015). This seems to be particularly evident particularly in the Viscount-Melville Sound and M'Clintock Channels regions when comparing 2009 (Figure 3a) with 2017 (Figure 3i) and 2018 (Figure 3j). Indeed, several studies have reported considerable decreases in the age and thickness of Arctic Ocean MYI north of the CAA in recent years (e.g. Kwok, 2018; Petty et al., 2020; Tschudi et al., 2020)

3.2 Comparison of RADARSAT-2 f_{pk} with Sentinel-1, *in situ*, and MODIS

Frequency distributions of RADARSAT-2 f_{pk} and Sentinel-1 f_{pk} from Scharien et al. (2017) in the CAA for 2016 and 2017 are shown in Figure 6. Sentinel-1 appears to estimate more regions of lower f_{pk} compared to RADARSAT-2 which are typically associated with MYI. Whereas, RADARSAT-2 estimates more regions of higher f_{pk} which are typically associated with smooth FYI. We consider these subtle differences to be primarily the result of taking the mean of all available April RADARSAT-2 imagery (Table 1) over all incidence angles in the CAA compared to only using images from Sentinel-1 within the CAA constrained to a certain incident angle range. As shown in Figure 2, the uncertainty in RADARSAT-2 f_{pk} varies depending on the number of pixel overlaps (images). Overall, the f_{pk} distributions are in good agreement between both sensors.

The *in situ* evolution of f_p over FYI within the CAA acquired by Landy et al. (2014) and illustrated in Figure 7a allows us to place the RADARSAT-2 f_{pk} estimates within the melt pond stages of development classification system. Unfortunately, no MODIS f_p observations are located in close proximity to the *in situ* observations. The evolution of melt ponds on the surface of the sea ice has been classified into four distinct and consecutive stages. A brief description is provided here, and the reader is referred to Eicken et al. (2004) and Polashenski et al. (2012) for a more comprehensive description. In stage I, meltwater from snow melt fills topographic depressions on the surface of the sea ice until the ponds reach their maximum areal extent. In stage II, melt pond coverage decreases due to horizontal water transport into macroscopic flaws and drainage through the ice. In stage III, the melt ponds typically drain through to the ocean and further changes in melt pond coverage depend on changes in surface topography and freeboard. Finally, in stage IV, melt ponds that survived the melt season refreeze and snow begins to accumulate on their surface.

Figure 7a compares the time series of the entire 100 m LiDAR melt pond fraction coincident with the f_{pk} determined from RADARSAT-2 at the coinciding pixels. For 2011, RADARSAT-2 f_{pk} corresponds to the end of stage I and beginning of stage II thus providing a very good representation of the seasonal peak of the f_p , when the melt pond control on heat uptake and ice decay, through the ice-albedo feedback, is greatest. For 2012, RADARSAT-2 f_{pk} also corresponds to the end of stage I and beginning of stage II but is ~ 0.2 lower than *in situ* f_p values. This is likely due to the short duration but very high maximum f_p of 0.78 in 2012 as Scharien et al. (2017) found that equation (1) sometimes underestimates very high f_p due to the low γ^p signal associated with very smooth FYI.

To give spatial context beyond the single point comparison at the LiDAR site, Figure 7b shows the distribution of RADARSAT-2 f_{pk} and the f_p determined from aerial photo observations on June 22nd, 2012 near Resolute. The aerial photographs were acquired within 1 week of f_{pk} coverage being observed at the LiDAR site. The comparison was done by averaging all RADARSAT-2 pixels within each aerial photo (123 photos) which represents ~ 861 samples. The mean aerial photograph f_p was 0.54 and RADARSAT-2 f_{pk} was 0.53 with an the RMSE of 0.10 and bias of 0. The distributions are in reasonably good agreement but RADARSAT-2 values are slightly narrower than the distribution of f_p from the aerial photographs. It is likely the RADARSAT-2 distribution is narrow on the left tail because our method captures peak pond

1 coverage and some of the regions photographed were before or after their seasonal peak. We attribute the narrow right tail to
2 the documented underestimation of equation (1) from Scharien et al. (2017). However, it is notable that both RADARSAT-2
3 and the aerial photograph datasets capture the same bimodal f_p distribution, with the first mode around 0.4-0.5 characterizing
4 rougher sea ice areas and the second mode around 0.7 capturing smooth flooded sea ice.

5 The seasonal time series of the 8-day composite MODIS f_p , the maximum seasonal MODIS f_p and the predicted
6 RADARSAT-2 f_{pk} for 2009-2011 is shown in Figure 8. MODIS f_p observations within the CAA indicate initial pond
7 formation occurred in May for all years with f_{pk} reached in mid-July for 2009 and in early June for 2010 and 2011.
8 Compared to the RADARSAT-2 f_{pk} values, the peak MODIS f_p is ~ 0.20 smaller. RADARSAT-2 f_{pk} is higher on average than
9 MODIS because the MODIS 8-day product does not represent f_{pk} . The MODIS f_p observations are determined weekly using
10 8-day composite image products that would include some melt pond formation and drainage processes prior-to, and after, the
11 seasonal peak. Moreover, MODIS f_p values are essentially aggregated from 500 m clear-sky pixels within a 12.5 km x 12.5
12 km grid cell (Rösel et al., 2012) and the 500 m spatial resolution may limit detection of smaller pond fractions as well as not
13 all of the 500 m pixels within the 12.5 km x 12.5 km grid cell are likely to be at the same melt pond stage evolution. Finally,
14 MODIS f_p observations give the time series of f_p therefore even the highest seasonal estimated MODIS f_p is reduced because
15 while some regions of the CAA are at their seasonal peak but others are behind or ahead. To that end, we also calculated the
16 maximum f_p from MODIS regardless of timing during the melt season, for each pixel, also shown in Figure 8. These values
17 more closely compare with the RADARSAT-2 f_{pk} but are still ~ 0.05 smaller on average. Even the maximum f_p from MODIS
18 is from an 8-day running mean of daily pond fraction estimates, so will underestimate the f_{pk} if the duration of peak ponding
19 is < 8 days. However, the top whisker of the box plot of the maximum f_p from MODIS indicates that MODIS does capture
20 some regions at peak during the 8-day time series. Although we are using MODIS f_p product to compare against our
21 RADARSAT-2 f_{pk} estimates, Rösel et al. (2012) found that the MODIS f_p product also has errors up to ~ 0.1 . Overall,
22 MODIS f_p estimates are more representative of the seasonal mean f_p rather than f_{pk} within the CAA.

23 24 **3.3 Influence of RADARSAT-2 f_{pk} on summer sea ice conditions**

25 In order to investigate if RADARSAT-2 f_{pk} values can be used to provide predictive information for summer sea ice
26 area within the CAA, we separated the CAA into numerous predefined subregions and then determined the detrended
27 correlations between RADARSAT-2 f_{pk} and weekly sea ice area from the CISDA regional ice charts in each region over the
28 period of 2009-2018. We tested each week from the start of June to the end of September. The strongest correlation, together
29 with the corresponding week of occurrence are shown in Figures 9a and 9b, respectively. All the strongest correlations are
30 negative, indicating – as expected – that years with higher predicted f_{pk} values are associated with lower sea ice area at a later
31 point in the summer. Higher f_{pk} lower the area-averaged albedo of the ice surface leading to accelerated melt and lower sea
32 ice concentrations (e.g. Perovich and Polashenski, 2012). There is considerable spatial variability in the strongest correlation
33 across the CAA with relatively low correlations in the majority of the northern CAA and very low correlations in the eastern
34 regions of the CAA. The regions of Kellet-Crozier ($R = -0.92$), Viscount-Melville Sound ($R = -0.73$), M'Clintock Channel

1 (R=-0.77) and Norwegian Bay (R=-0.78) all exhibit statistically significant correlations above the 95% confidence level. In
2 terms of timing for the statistically significant regions, RADARSAT-2 f_{pk} correlated the strongest to weekly sea ice area in
3 August for all regions except Norwegian Bay (Figure 9b). Compared to previous studies, the primary difference between
4 using f_p values to predict summer sea ice conditions seems to be the timing of when the correlation is the strongest. Using
5 simulated f_p values, Schröder et al. (2014) found the strongest correlation to September sea ice occurred for the May f_p . Liu
6 et al. (2015) used observed MODIS f_p values and reported the strongest correlation to September sea ice in late July. Our
7 findings suggest that methods such as these may be able to predict August sea ice area from f_{pk} simulations or observations
8 with higher confidence than September ice area, at least in the CAA.

9 Why is the relationship stronger in some regions of the CAA and weaker in others? RADARSAT-2 f_{pk} values are
10 determined from imagery acquired in April when ice conditions in the CAA are landfast (immobile) and do not evolve in
11 concert with sea ice dynamics operating within the CAA. As a result, RADARSAT-2 f_{pk} values will not be spatially
12 representative of the region's ice conditions when region-specific dynamic breakup processes dominate over
13 thermodynamics (i.e. *in situ* melt). In other words, the origin of ~~the some of~~ the ice in these regions during the summer melt
14 season will be not always be the same as in April (i.e. pre-melt) when the initial RADARSAT-2 f_{pk} value was determined.
15 The time series of weekly detrended RADARSAT-2 f_{pk} and weekly sea ice area for selected regions within the CAA is
16 shown in Figure 10 and provides evidence for this regional dichotomy. In the Viscount-Melville Sound and M'Clintock
17 regions the correlations gradually get stronger, reaching a peak in August. These regions are known to be immobile and
18 stagnant (e.g. Melling, 2002) with the majority of breakup taking place in September which is when the relationship begins
19 to degrade. The Kellet-Crozier is another stagnant region which supports that in the absence of considerable ice dynamics
20 the relationship between RADARSAT-2 f_{pk} and sea ice area is strong throughout the melt season. The time series in Penny
21 Strait illustrates how the correlation gradually increase but when the region's dynamic break-up begins in July, ice is
22 advected southward which degrades the correlation. This was also the case for other many regions in the northern CAA (not
23 shown) as the flushing of sea ice southward from the northern CAA is a regular occurrence during the melt season (Melling,
24 2002; Howell et al., 2006). The low correlations in the south eastern regions of the CAA are also likely a function of ice
25 dynamics as these regions of the CAA are known to be considerably influenced by currents and wind (Prinsenber and
26 Hamilton, 2005) and sea ice speed in Lancaster Sound and Barrow Strait can reach 10 km day⁻¹ (Agnew et al., 2008).

27 The strong and statistically significant correlation in the Viscount-Melville Sound region is encouraging as it is a
28 key shipping region in the northern route of the Northwest Passage. To that end, we used linear regression to predict mean
29 August sea ice area within Viscount-Melville Sound with the detrended RADARSAT-2 f_{pk} values as a predictor. Figure 11
30 illustrates the results as compared to observations (detrended) from the CISDA ice charts for 2009-2018. There is reasonable
31 agreement between the predicted and observed sea ice area in the region with an RMSE of 18×10^3 km² and an $R^2=0.44$. The
32 largest discrepancies occurred for 2013 and 2014 with the RADARSAT-2 f_{pk} model prediction resulting in too little sea ice
33 area. Overall, within the Viscount-Melville Sound region of CAA there is a period for which a significant statistical
34 relationship exists between RADARSAT-2 f_{pk} and the summer ice area before sea ice dynamics degrades the relationship.

1
2
3
4
5
6
7
8
9
10
11
12
13
14
15
16
17
18
19
20
21
22
23
24
25
26
27
28
29
30
31
32
33
34

4 Conclusions

In this study we predicted and analyzed spring f_{pk} using RADARSAT-2 within the CAA from 2009-2018. The spatial variability in RADARSAT-2 f_{pk} was found to be excellent agreement with the spatial distribution of sea ice stage of development prior to the melt season as high (low) f_{pk} values were associated with FYI (MYI) types. The temporal variability of RADARSAT-2 f_{pk} over the 10-year record was significantly correlated to April MYI area, highlighting the importance of MYI within the CAA. RADARSAT-2 f_{pk} was found to be in good agreement with the f_{pk} maximum extent observed *in situ* for 2011 but were slightly lower than 2012 when peak f_p was very large (> 0.7). Compared to peak MODIS f_p values, RADARSAT-2 f_{pk} values were larger by ~ 0.05 . Based on our comparative analysis, RADARSAT-2 f_{pk} is more representative of peak f_p within the CAA compared to the MODIS 8-day product which on average was found to underestimate f_{pk} by ~ 0.2 and is more representative of the seasonal mean f_p . We also found ~~to be in~~ excellent agreement between RADARSAT-2 and Sentinel-1 which suggests that combining both Sentinel-1 and the recently launched RADARSAT Constellation Mission (RCM) could facilitate pan-Arctic f_{pk} estimates. The RCM will also facilitate continued investigation of additional metrics that when combined with γ° could further improve predicted f_{pk} .

The results presented in this study indicate that dynamically stable sea ice regions within the CAA exhibit a higher detrended correlation between RADARSAT-2 f_{pk} and summer sea ice area. Specifically, the strong and statistically significant de-trended correlation in the Viscount-Melville Sound region demonstrates that RADARSAT-2 f_{pk} estimates are useful for providing predictive information about summer sea ice area in the northern route of the Northwest Passage. This information could find utility in constraining regional model simulations (e.g. Lemieux et al., 2016). Alternatively, it could be advantageous to exploit the high spatial resolution of SAR and investigate if local-scale f_{pk} estimates could enhanced knowledge of summer ice conditions in northern communities (e.g. Cooley et al., 2020). Ultimately, imagery from RCM will ensure our time series of RADARSAT-2 f_{pk} estimates in the CAA will continue, gradually building statistics facilitating the development of more robust statistical relationships in upcoming years.

Data Availability

RADARSAT-2 imagery is available online for a fee from the Earth Observation Data Management System (<https://www.eodms-sgdot.nrcan-rncan.gc.ca>). RADARSAT-2 derived melt pond fraction is available through the lead author SELH (stephen.howell@canada.ca). MODIS Arctic melt pond cover fractions dataset available from the Integrated Climate Data Center (ICDC, <https://icdc.cen.uni-hamburg.de/>). The CISDA is available online from the Canadian Ice Service (CIS; <https://www.canada.ca/en/environment-climate-change/services/ice-forecasts-observations/latest-conditions/archive-overview.html>). *In situ* melt pond data is available through contributing author JL (jack.landy@bristol.ac.uk) and the melt pond aerial photograph data is available through contributing author RLS (randy@uvic.ca).

1 **Author contributions**

2 SELH wrote the manuscript with input from all authors. SELH and MB preformed the analysis.

3

4 **Competing interests**

5 The authors declare that they have no conflict of interest.

6

7 **Acknowledgements**

8 Funding for RKS provided by Polar Knowledge Canada Science and Technology Program Grant NST-1718-0024 and
9 Marine Environmental Observation Prediction and Response Network (MEOPAR) project 1-02-02-012.5. JL is supported by
10 the European Space Agency Living Planet Fellowship “Arctic-SummIT” under Grant ESA/4000125582/18/I-NS and the
11 Natural Environment Research Council Grants “PRE-MELT” NE/T000546/1 and “Diatom-ARCTIC” NE/R012849/1.

12 **References**

13 Agnew, T., Lambe, A., and Long, D.: Estimating sea ice area flux across the Canadian Arctic Archipelago using enhanced
14 AMSR-E, *Journal of Geophysical Research.*, 113, C10011, doi:10.1029/2007JC004582, 2008.

15

16 Chevallier, M., Salas, D., Méliá, Y., Voldoire, A., Déqué, M., and Garric, G.: Seasonal forecasts of the pan-Arctic sea ice
17 extent using a GCM-based seasonal prediction system, *Journal of Climate*, 26, 6092–6104, doi:10.1175/JCLI-D-12-00612.1,
18 2013

19

20 Cooley, S.W., Ryan, J.C., Smith, L.C. et al.: Coldest Canadian Arctic communities face greatest reductions in shorefast sea
21 ice. *Nature Climate Change*. <https://doi.org/10.1038/s41558-020-0757-5>, 2020.

22

23 Dumas, J. A., Flato, G.M., and Brown, R.D.: Future projections of landfast ice thickness and duration in the Canadian
24 Arctic, *Journal of Climate*, 19, 5175–5189, 2006.

25

26 Eicken, H.: Ocean science: Arctic sea ice needs better forecasts, *Nature*, 497(7450), 431–433, doi:10.1038/497431a, 2013.

27

28 Eicken, H., Krouse, H.R., Kadko, D., Perovich, D.K.: Tracer studies of pathways and rates of meltwater transport through
29 Arctic summer sea ice, *Journal of Geophysical Research*, 107(C10), 8046, doi:10.1029/2000JC000583, 2002.

30

31 Eicken, H., Grenfell, T.C., Perovich, D.K., Richter-Menge, J.A., and Frey, K.: Hydraulic controls of summer Arctic pack ice
32 albedo, *Journal of Geophysical Research*, 109, C08007, doi:10.1029/2003JC001989, 2004.

33

34 Flocco, D., Feltham, D.L., and Turner, A.K.: Incorporation of a physically based melt pond scheme into the sea ice
35 component of a climate model, *Journal of Geophysical Research*, 115, C08012, doi:10.1029/2009JC005568, 2010.

36

37 Flocco, D., Schröder, D., Feltham, D.L. and Hunke, E.C.: Impact of melt ponds on Arctic sea ice simulations from 1990 to
38 2007, *Journal of Geophysical Research*, 117, C09032, doi:10.1029/2012JC008195, 2012.

39

40 Fors, A. S., Divine, D. V., Doulgeris, A. P., Renner, A. H. H., and Gerland, S.: Signature of Arctic first-year ice melt pond
41 fraction in X-band SAR imagery, *The Cryosphere*, 11, 755–771, <https://doi.org/10.5194/tc-11-755-2017>, 2017.

42

1 Grenfell, T. C., and Perovich, D.K.: Seasonal and spatial evolution of albedo in a snow-ice-land-ocean environment, *Journal*
2 *of Geophysical Research*, 109, C01001, doi:10.1029/2003JC001866, 2004.
3

4 Guemas, V., Chevallier, M., Déqué, M., Bellprat, O., Doblus-Reyes, F.: Impact of sea ice initialization on sea ice and
5 atmosphere prediction skill on seasonal timescales, *Geophysical Research Letters*, 43, 3889–3896,
6 doi:10.1002/2015GL066626, 2016.
7

8 Howell, S.E.L., Tivy, A., Yackel, J.J., and Scharien, R.K.: Application of a SeaWinds/QuikSCAT sea ice melt algorithm for
9 assessing melt dynamics in the Canadian Arctic Archipelago. *Journal of Geophysical Research-Oceans*, 111, C07025,
10 doi:10.1029/2005JC003193, 2006.
11

12 Howell, S. E. L., Wohlleben, T., Komarov, A., Pizzolato, L., and Derksen, C.: Recent extreme light sea ice years in the
13 Canadian Arctic Archipelago: 2011 and 2012 eclipse 1998 and 2007, *The Cryosphere*, 7, 1753–1768,
14 <https://doi.org/10.5194/tc-7-1753-2013>, 2013.
15

16 Howell, S. E. L., Laliberté, F., Kwok, R., Derksen, C., and King, J.: Landfast ice thickness in the Canadian Arctic
17 Archipelago from observations and models, *The Cryosphere*, 10, 1463–1475, <https://doi.org/10.5194/tc-10-1463-2016>, 2016.
18

19 Howell, S. E. L., and Brady, M.: The dynamic response of sea ice to warming in the Canadian Arctic Archipelago.
20 *Geophysical Research Letters*, 46, 13119– 13125. <https://doi.org/10.1029/2019GL085116>, 2019
21

22 Hu, X., Sun, J., Chan, T. O., and Myers, P. G.: Thermodynamic and dynamic ice thickness contributions in the Canadian
23 Arctic Archipelago in NEMO-LIM2 numerical simulations, *The Cryosphere*, 12, 1233–1247, [https://doi.org/10.5194/tc-12-](https://doi.org/10.5194/tc-12-1233-2018)
24 [1233-2018](https://doi.org/10.5194/tc-12-1233-2018), 2018.
25

26 Istomina, L., Heygster, G., Huntemann, M., Schwarz, P., Birnbaum, G., Scharien, R., Polashenski, C., Perovich, D., Zege,
27 E., Malinka, A., Prikhach, A., and Katsev, I.: Melt pond fraction and spectral sea ice albedo retrieval from MERIS data –
28 Part 1: Validation against in situ, aerial, and ship cruise data, *The Cryosphere*, 9, 1551–1566, [https://doi.org/10.5194/tc-9-](https://doi.org/10.5194/tc-9-1551-2015)
29 [1551-2015](https://doi.org/10.5194/tc-9-1551-2015), 2015.
30

31 Kwok, R.: Arctic sea ice thickness, volume, and multiyear ice coverage: losses and coupled variability (1958–2018).
32 *Environmental Research Letters*, 13, 105005, doi:10.1088/1748-9326/aae3ec, 2018.
33

34 Laliberté, F., Howell, S.E.L. and Kushner, P.J.: Regional variability of a projected sea ice-free Arctic during the summer
35 months, *Geophysical Research Letters*, 43, doi:10.1002/2015GL066855, 2016.
36

37 Laliberté, F., Howell, S. E. L., Lemieux, J.-F., Dupont, F., and Lei, J.: What historical landfast ice observations tell us about
38 projected ice conditions in Arctic archipelagoes and marginal seas under anthropogenic forcing, *The Cryosphere*, 12, 3577–
39 3588, <https://doi.org/10.5194/tc-12-3577-2018>, 2018.
40

41 Landy, J.C., Ehn, J.K., Shields, M. and Barber, D.G.: Surface and melt pond evolution on landfast first-year sea ice in the
42 Canadian Arctic Archipelago, *Journal of Geophysical Research*, 119(5), 3054-3075, 2014.
43

44 Landy, J.C., Ehn, J.K., and Barber, D.G.: Albedo feedback enhanced by smoother Arctic sea ice, *Geophysical Research*
45 *Letters*, 42(24), 710-714. doi:10.1002/2015GL066712, 2015.
46

47 Lee, S., Stroeve, J.C., Tsamados, M. and Khand, A.L.: Machine learning approaches to retrieve pan-Arctic melt ponds from
48 visible satellite imagery, *Remote Sensing of Environment*, <https://doi.org/10.1016/j.rse.2020.111919>, 2020.
49

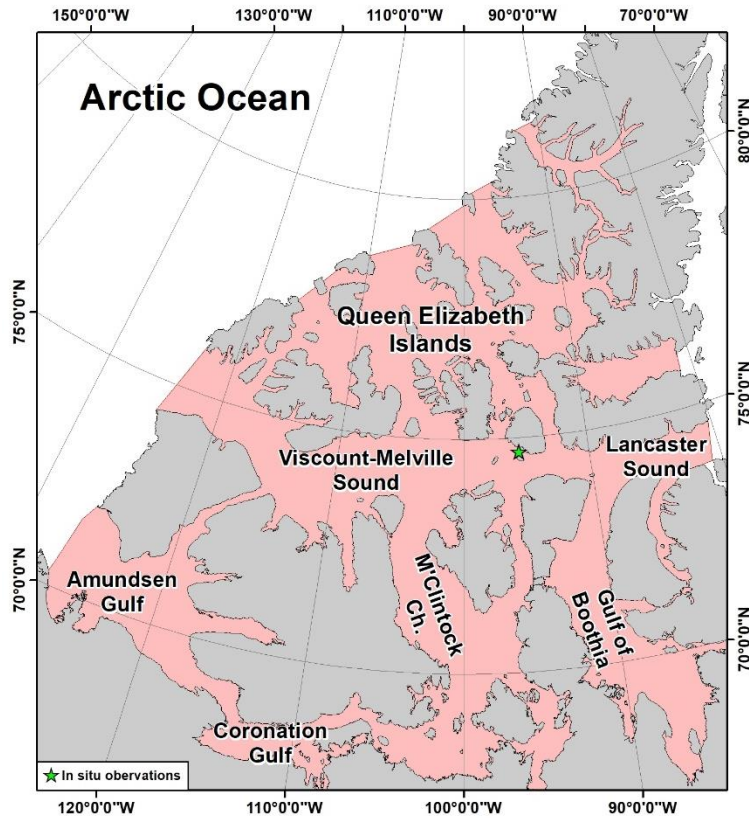
1 Lemieux, J.-F., Beaudoin, C., Dupont, F., Roy, F., Smith, G.C., Shlyayeva, A., Buehner, M., Caya, A., Chen, J., Carrieres, T.,
2 Pogson, L., DeRepentigny, P., Plante, A., Pestieau, P., Pellerin, P., Ritchie, H., Garric, G. and Ferry, N.: The Regional Ice
3 Prediction System (RIPS): verification of forecast sea ice concentration. *Q.J.R. Meteorol. Soc.*, 142: 632-643.
4 doi:10.1002/qj.2526, 2016.
5
6 Li, H., Perrie, W., Li, Q., and Hou, Y.: Estimation of melt pond fractions on first year sea ice using compact polarization
7 SAR. *Journal of Geophysical Research*, 122, 8145–8166, <https://doi.org/10.1002/2017JC013248>, 2017.
8
9 Liu, J., Song, M.H., Horton R.M., and Hu, Y.: Revisiting the potential of melt pond fraction as a predictor for the seasonal
10 Arctic sea ice extent minimum, *Environmental Research Letters*, 10(5). <https://doi.org/10.1088/1748-9326/10/5/054017>,
11 2015.
12
13 Markus, T., Cavalieri, D.J., Tschudi, M.A., and Ivanoff, A.: Comparison of aerial video and Landsat 7 data over ponded sea
14 ice, *Remote Sensing of Environment*, 86, 458–469, 2003.
15
16 Maslanik, J., Stroeve, J., Fowler, C., and Emery, W.: Distribution and trends in Arctic sea ice age through spring 2011,
17 *Geophysical Research Letters*, 38, L13502, doi:10.1029/2011GL047735, 2011.
18
19 Peng, G. and Meier, W.M.: Temporal and regional variability of Arctic sea-ice coverage from satellite data, *Annals of*
20 *Glaciology*, 59(76pt2), 191-200. doi:10.1017/aog.2017.32, 2017.
21
22 Perovich, D. K., Grenfell, T.C., Light, B., and Hobbs, P.V.: Seasonal evolution of the albedo of multiyear Arctic sea ice,
23 *Journal of Geophysical Research*, 107(C10), 8044, doi:10.1029/2000JC000438, 2002.
24
25 Petty, A. A., Kurtz, N.T., Kwok, R., Markus, T., and Neumann, T. A.: Winter Arctic sea ice thickness from ICESat-2
26 freeboards. *Journal of Geophysical Research: Oceans*, 125, e2019JC015764. <https://doi.org/10.1029/2019JC015764>, 2020.
27
28 Perovich, D. K., and Polashenski., C.: Albedo evolution of seasonal Arctic sea ice, *Geophysical Research Letters*, 39,
29 L08501, doi:10.1029/2012GL051432, 2012.
30
31 Pizzolato, L., Howell, S.E.L., Derksen, C., Dawson, J., and Copland, L.: Changing sea ice conditions and marine
32 transportation activity in Canadian Arctic waters between 1990 and 2012, *Climatic Change*, 123, 161–173,
33 doi:10.1007/s10584-013-1038-3, 2014.
34
35 Polashenski, C., Perovich, D.K., and Courville, Z.: The mechanisms of sea ice melt pond formation and evolution, *Journal of*
36 *Geophysical Research*, 117, C01001, doi:10.1029/2011JC007231, 2012.
37
38 Prinsenberg, S.J and Hamilton, J.: Monitoring the volume, freshwater and heat fluxes passing through Lancaster sound in the
39 Canadian Arctic Archipelago, *Atmosphere-Ocean*, 43:1, 1-22, DOI: 10.3137/ao.430101, 2005.
40
41 Rösel, A., Kaleschke, L., and Birnbaum, G.: Melt ponds on Arctic sea ice determined from MODIS satellite data using an
42 artificial neural network, *The Cryosphere*, 6(2), 431–446. <https://doi.org/10.5194/tc-6-431-2012>, 2012.
43
44 Scharien, R. K., Hochheim, K., Landy, J., and Barber, D.G.: First-year sea ice melt pond fraction estimation from dual-
45 polarisation C-band SAR – Part 2: Scaling in situ to Radarsat-2, *The Cryosphere*, 8, 2163-2176, [https://doi.org/10.5194/tc-8-](https://doi.org/10.5194/tc-8-2163-2014)
46 2163-2014, 2014.
47
48 Scharien, R. K., Segal, R., Nasonova, S., Nandan, V., Howell, S.E.L. and Haas, C.: Winter Sentinel-1 backscatter as a
49 predictor of spring Arctic sea ice melt pond fraction. *Geophysical Research Letters*, 44,
50 <https://doi.org/10.1002/2017GL075547>, 2017.

1
2 Serreze, M.C., Holland, M.M. and Stroeve, J.: Perspectives on the Arctic's shrinking sea-ice cover, *Science*, 315: 1533-1536,
3 2007.
4
5 Schröder, D., Feltham, D. L., Flocco, D., and Tsamados, M.: September Arctic sea-ice minimum predicted by spring melt-
6 pond fraction, *Nature Climate Change*, 4(5), 353–357. <https://doi.org/10.1038/nclimate2203>, 2014.
7
8 Sigmond, M., Fyfe, J.C., Flato, G.M., Kharin, V.V. and Merryfield, W.J.: Seasonal forecast skill of Arctic sea ice area in a
9 dynamical forecast system, *Geophysical Research Letters*, 40, 529–534, doi:10.1002/grl.50129, 2013.
10
11 Small, D.: Flattening gamma: Radiometric terrain correction for SAR imagery, *IEEE Transactions on Geoscience and*
12 *Remote Sensing*, 49(8), 3081–3093. <https://doi.org/10.1109/TGRS.2011.2120616>, 2011.
13
14 Sou, T. and Flato, G.: Sea ice in the Canadian Arctic Archipelago: Modeling the past (1950–2004) and the future (2041–60),
15 *Journal of Climate*, 22, 2181–2198, 2009.
16
17 Stroeve, J. C., Serreze, M.C., Holland, M.M., Kay, J.E., Maslanik, J., and Barrett, A.P.: The Arctic’s rapidly shrinking sea
18 ice cover: A research synthesis, *Climatic Change*, 110(3–4), 1005–1027, doi:10.1007/s10584-011-0101-1, 2012.
19
20 Tivy, A., Howell, S.E.L., Alt, B., McCourt, S., Chagnon, R., Crocker, G., Carrieres, T., and Yackel, J.J.: Trends and
21 variability in summer sea ice cover in the Canadian Arctic based on the Canadian Ice Service Digital Archive, 1960–2008
22 and 1968–2008, *Journal of Geophysical Research*, 116, C03007, doi:10.1029/2009JC005855, 2011.
23
24 Tschudi, M. A., Maslanik, J.A., and Perovich, D.K.: Derivation of melt pond coverage on arctic sea ice using MODIS
25 observation, *Remote Sensing of Environment*, 112, 2605–2614, 2008.
26
27 Tschudi, M. A., Meier, W. N., and Stewart, J. S.: An enhancement to sea ice motion and age products at the National Snow
28 and Ice Data Center (NSIDC), *The Cryosphere*, 14, 1519–1536, <https://doi.org/10.5194/tc-14-1519-2020>, 2020.
29
30 Webster, M. A., Rigor, I.G., Perovich, D.K., Richter-Menge, J.A., Polashenski, C.M. and Light, B.: Seasonal evolution of
31 melt ponds on Arctic sea ice, *Journal of Geophysical Research*, 120, 5968–5982, doi:10.1002/2015JC011030, 2015.
32
33
34
35
36
37
38
39
40
41
42
43
44

1
2
3
4
5
6
7
8
9
10
11
12
13
14
15
16
17

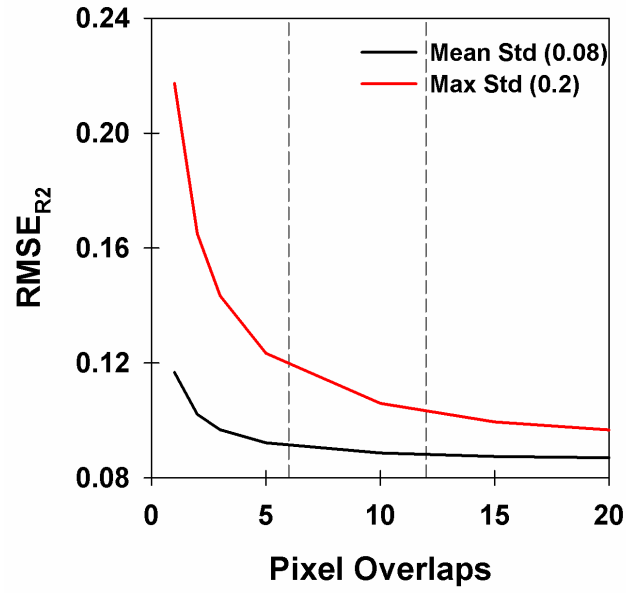
Table 1. Number of RADARSAT-2 images acquired over the Canadian Arctic Archipelago in April for 2009-2018.

Year	RADARSAT-2 Image Count
2009	90
2010	138
2011	149
2012	149
2013	188
2014	159
2015	133
2016	159
2017	151
2018	144



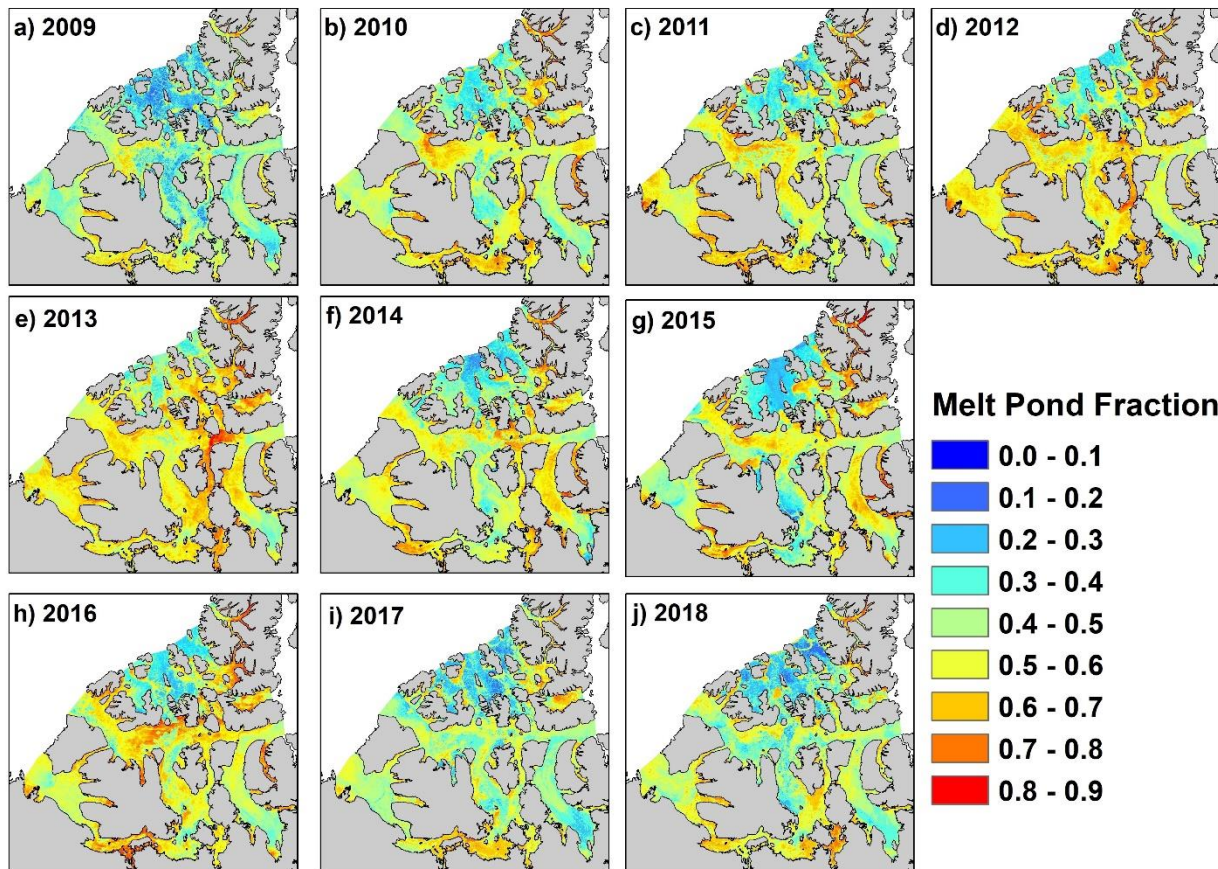
1
2
3
4
5
6
7
8
9
10
11

Figure 1. Map of the Canadian Arctic Archipelago region (red shading). The green star indicates the location of the LiDAR and aerial photograph observations.



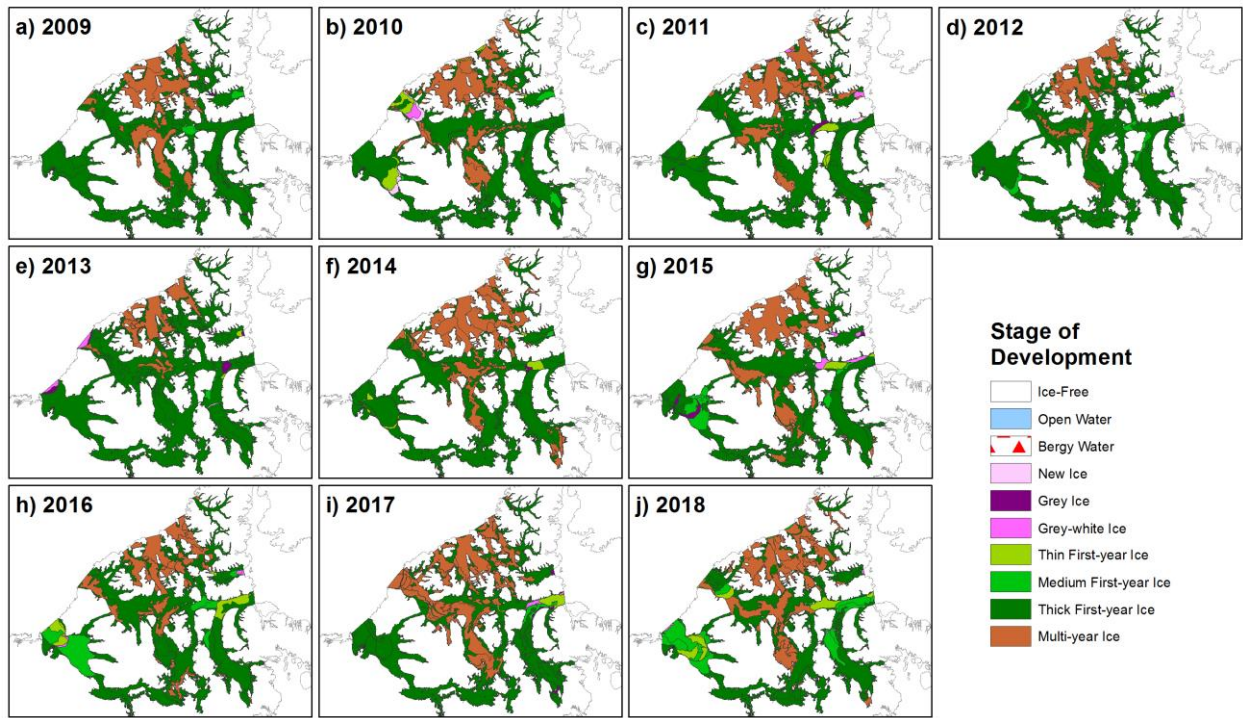
1
2
3
4
5
6
7
8
9

Figure 2. The root-mean square error of RADARSAT-2 peak melt pond fraction values (RMSE_{R2}) with increasing number of RADARSAT-2 pixel overlaps. The vertical dashed lines indicate the range of typical overlap from 2009-2018.



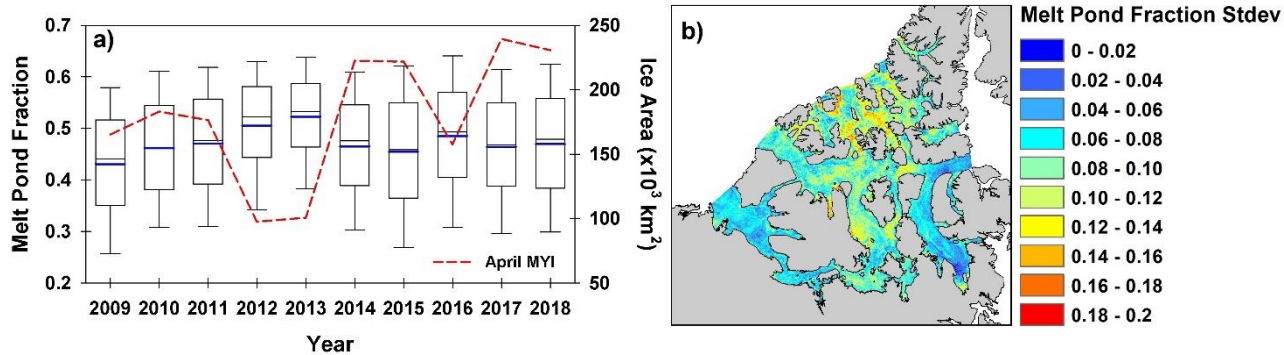
1
2
3
4
5

Figure 3. Spatial distribution of RADARSAT-2 peak melt pond fraction (f_{pk}) in the Canadian Arctic Archipelago from 2009-2018 (a-j).

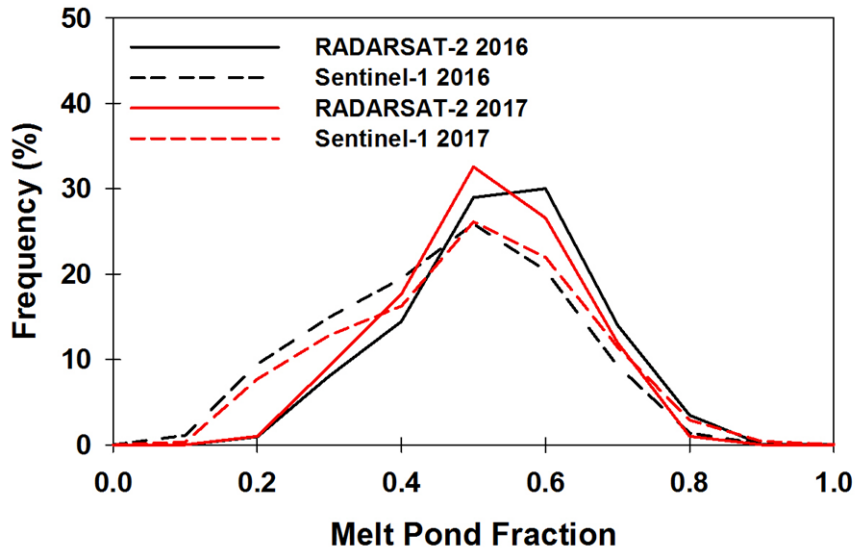


1
2 **Figure 4.** Spatial distribution of sea ice stage of development (type) on the first week of April in the Canadian Arctic Archipelago for
3 2009-2018 (a-j).

4
5
6
7
8
9
10
11
12
13
14
15
16

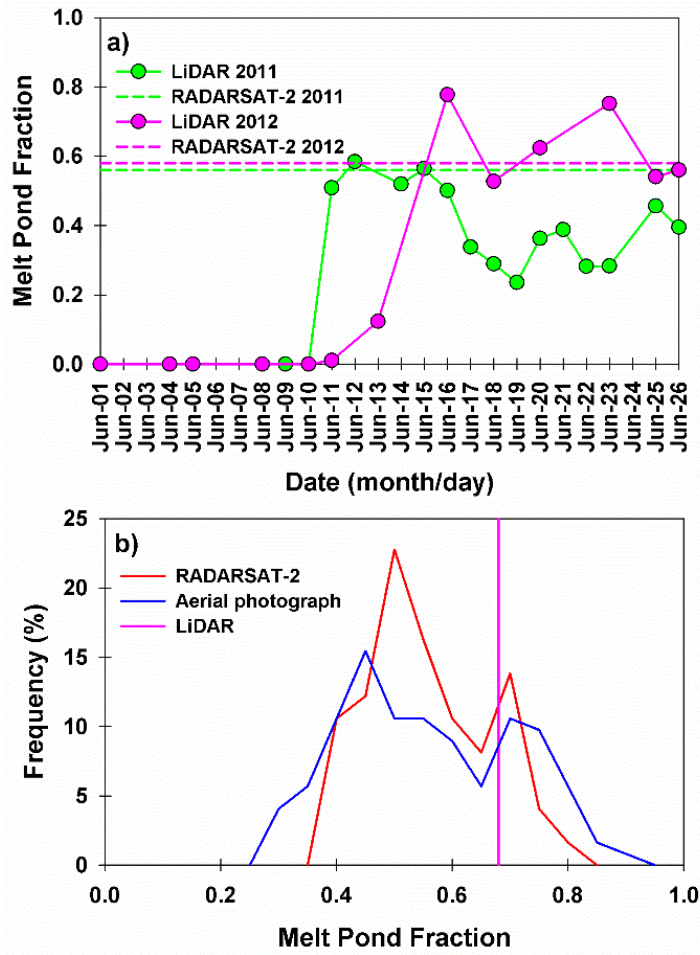


1
 2 **Figure 5.** Boxplot time series of RADARSAT-2 peak melt pond fraction (f_{pk}) and mean April multi-year ice (MYI) area in the Canadian
 3 Arctic Archipelago for 2009-2018. The solid blue line represents the mean (a). Spatial distribution of the RADARSAT-2 f_{pk} standard
 4 deviation from 2009-2018 (b).

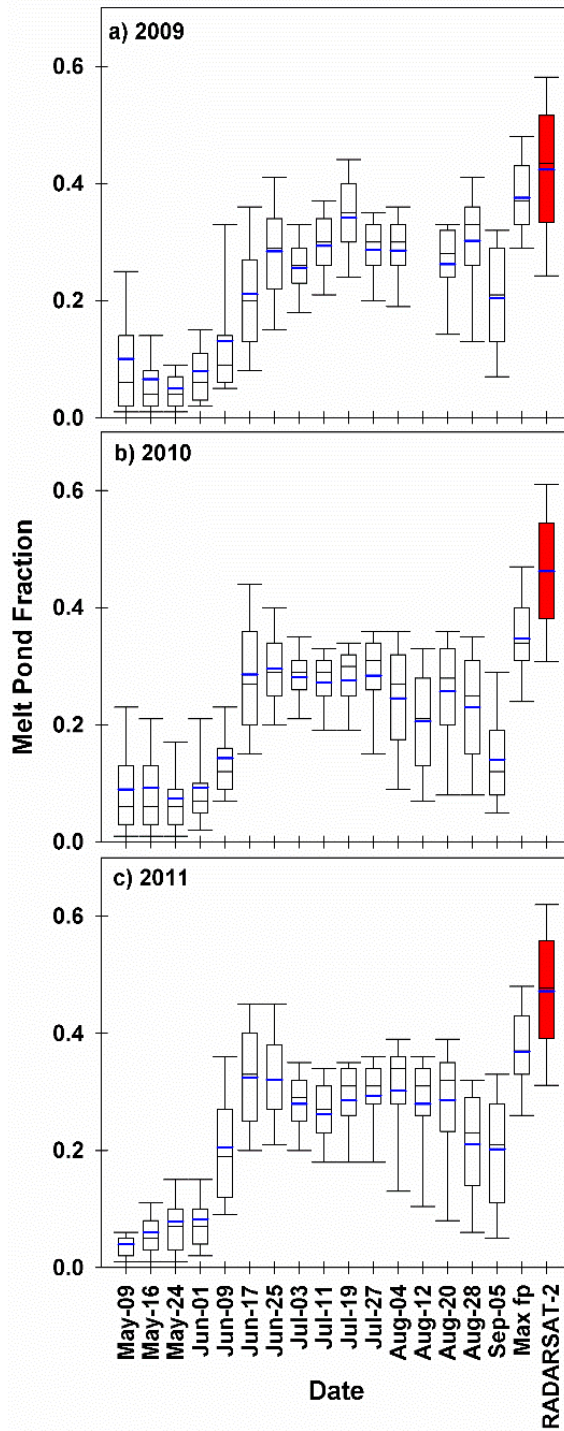


1
2
3
4
5
6
7
8
9
10
11
12
13
14
15
16
17

Figure 6. Frequency distribution (%) of RADARSAT-2 peak melt pond fraction (f_{pk}) and Sentinel-1 f_{pk} from Scharien et al. (2017) in the Canadian Arctic Archipelago for 2016 and 2017.

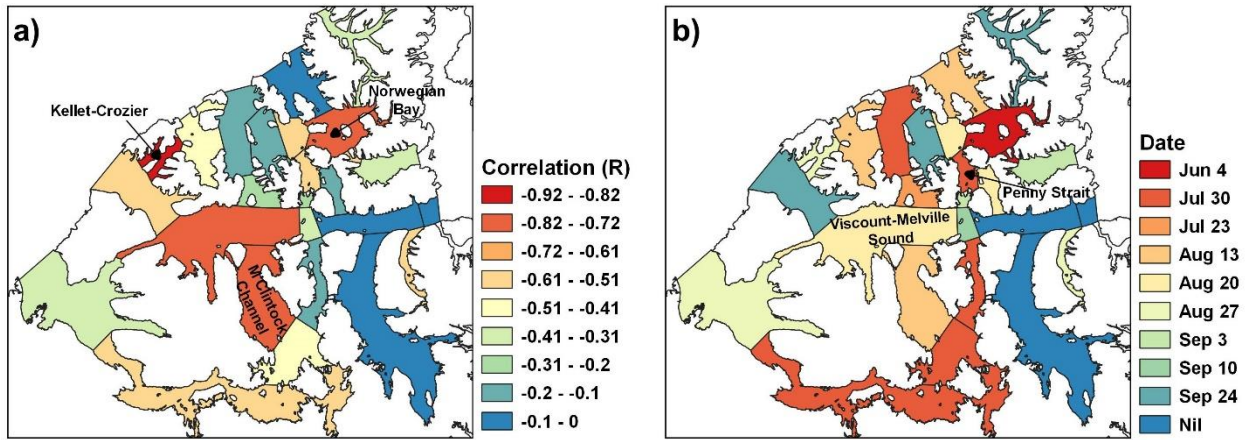


1
 2 **Figure 7.** a) Temporal evolution of observed melt pond fraction (f_p) and RADARSAT-2 peak melt pond fraction (f_{pk}) at *in*
 3 *situ* observations sites for 2011 (74.7229°N; 95.1763°W) and 2012 (74.7264°N; 95.5772°W). b) Frequency distribution of
 4 RADARSAT-2 f_{pk} and aerial photograph f_p observations in Resolute Passage on June 22, 2012; the pink vertical link
 5 represents the mean LiDAR f_p on June 22, 2012.

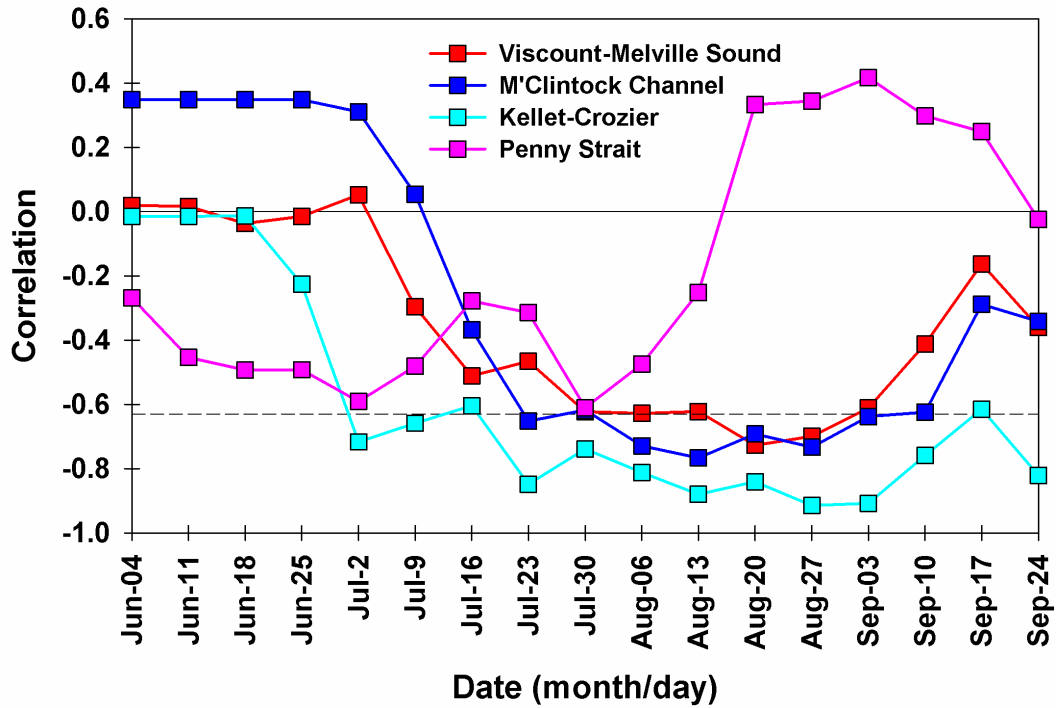


1

2 **Figure 8.** Boxplots of the seasonal time series of MODIS melt pond fraction (f_p), the maximum seasonal MODIS f_p and RADARSAT-2
 3 peak melt pond fraction (f_{pk}) for (a) 2009, (b) 2010 and (c) 2011. The solid blue line represents the mean.

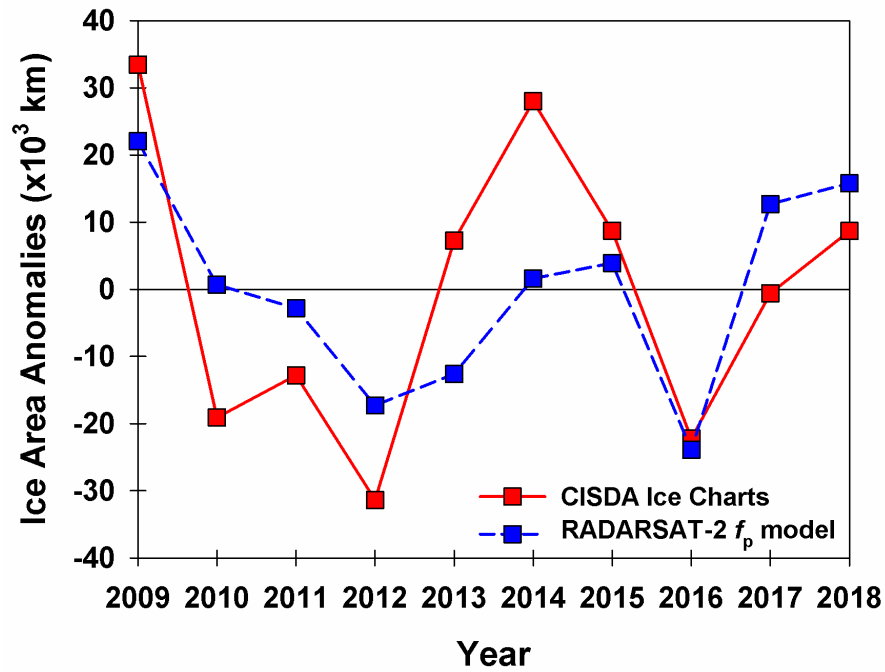


1
2 **Figure 9.** Spatial distribution of the (a) strongest detrended correlation (R) between RADARSAT-2 peak melt pond fraction (f_{pk}) and
3 weekly sea ice area and (b) week of occurrence.



1
2
3
4
5
6
7
8
9

Figure 10. Time series of detrended correlations between RADARSAT-2 peak melt pond fraction (f_{pk}) and weekly sea ice area for selected regions in the Canadian Arctic Archipelago from June to September. The dashed black line is statistical significance at the 95% confidence level.



1
 2 **Figure 11.** Predicated sea ice area anomalies (detrended) using RADARSAT-2 peak melt pond fraction (f_{pk}) and observed sea ice area
 3 anomalies (detrended) from the Canadian Ice Service Digital Archive (CISDA) ice charts in the Viscount-Melville Sound region of the
 4 Canadian Arctic Archipelago, 2009-2018.